Journal of Statistical Physics, Vol. 119, Nos. 3/4, May 2005 (© 2005)
DOI: 10.1007/s10955-005-3022-4

Airy Distribution Function: From the Area Under a Brownian Excursion to the Maximal Height of Fluctuating Interfaces

Satya N. Majumdar[1,2] **and Alain Comtet**[2,3]

Received September 20, 2004; accepted January 18, 2005

The Airy distribution function describes the probability distribution of the area under a Brownian excursion over a unit interval. Surprisingly, this function has appeared in a number of seemingly unrelated problems, mostly in computer science and graph theory. In this paper, we show that this distribution function also appears in a rather well studied physical system, namely the fluctuating interfaces. We present an exact solution for the distribution $P(h_m, L)$ of the maximal height h_m (measured with respect to the average spatial height) in the steady state of a fluctuating interface in a one dimensional system of size L with both periodic and free boundary conditions. For the periodic case, we show that $P(h_m, L) = L^{-1/2} f\left(h_m L^{-1/2}\right)$ for all $L > 0$ where the function $f(x)$ is the Airy distribution function. This result is valid for both the Edwards–Wilkinson (EW) and the Kardar–Parisi–Zhang interfaces. For the free boundary case, the same scaling holds $P(h_m, L) = L^{-1/2} F\left(h_m L^{-1/2}\right)$, but the scaling function $F(x)$ is different from that of the periodic case. We compute this scaling function explicitly for the EW interface and call it the F-Airy distribution function. Numerical simulations are in excellent agreement with our analytical results. Our results provide a rather rare exactly solvable case for the distribution of extremum of a set of *strongly correlated* random variables. Some of these results were announced in a recent Letter [S.N. Majumdar and A. Comtet, Phys. Rev. Lett. **92**: 225501 (2004)].

KEY WORDS: Brownian excursion; fluctuating interfaces; Airy distribution.

[1]Laboratoire de Physique Théorique (UMR C5152 du CNRS), Université Paul Sabatier, 31062 Toulouse Cedex, France.
[2]Laboratoire de Physique Théorique et Modèles Statistiques, Université Paris-Sud. Bât. 100. 91405 Orsay Cedex, France; e-mail: majumdar@ipno.in2p3.fr
[3]Institut Henri Poincaré, 11 rue Pierre et Marie Curie, 75005 Paris, France.

1. INTRODUCTION

A Brownian excursion $x(\tau)$ is a conditioned one dimensional Brownian motion over the time interval $0 \leqslant \tau \leqslant T$ such that its path starts and ends at the origin $x(0) = x(T) = 0$, but is constrained to stay positive in between (see Fig. 2). The area under the excursion, $A = \int_0^T x(\tau) d\tau$, is clearly a random variable taking a different value for each realization of the excursion. A natural question that the mathematicians have studied quite extensively over the past two decades is: what is the probability distribution $P(A, T)$ of the area under a Brownian excursion over the interval $[0, T]$? Since the typical lateral displacement of the excursion at time τ scales as $\sqrt{\tau}$, it follows that one can trivially rescale $x(\tau) = \sqrt{T} y(\tau/T)$ where $y(u)$ represents a Brownian excursion over the unit interval $u \in [0, 1]$. Hence, the area $A = \int_0^T x(\tau) d\tau \equiv T^{3/2} \int_0^1 y(u) du$ scales as $T^{3/2}$. Thus the area distribution has a scaling form, $P(A, T) = T^{-3/2} f\left(A/T^{3/2}\right)$. The normalization condition $\int_0^\infty P(A, T) dA = 1$ demands a prefactor $T^{-3/2}$ and also the conditions: $f(x) \geqslant 0$ for all x and $\int_0^\infty f(x) dx = 1$. One then interprets the scaling function $f(x)$ as the distribution of the area under the Brownian excursion $y(u)$ over a *unit* interval $u \in [0, 1]$. The function $f(x)$, or rather its Laplace transform, was first computed analytically by Darling[1] and Louchard,[2]

$$\tilde{f}(s) = \int_0^\infty f(x) e^{-sx} dx = s\sqrt{2\pi} \sum_{k=1}^{\infty} e^{-\alpha_k s^{2/3} 2^{-1/3}}, \tag{1}$$

where α_k's are the magnitudes of the zeros of the standard Airy function $Ai(z)$ on the negative real axis. For example, $\alpha_1 = 2.3381\ldots$, $\alpha_2 = 4.0879\ldots$, $\alpha_3 = 5.5205\ldots$ etc. Since the expression of $f(x)$ involves the zeros of Airy function, the function $f(x)$ has been named the Airy distribution function, which should not be confused with the Airy function $Ai(x)$ itself. Even though the Eq. (1) provides a formally exact expression of the Laplace transform, it turns out the calculation of the moments $M_n = \int_0^\infty x^n f(x) dx$ is highly nontrivial and they can be determined only recursively[3] (see Section 2). Takacs was also able to formally invert the Laplace transform in Eq. (1) to obtain,[3]

$$f(x) = \frac{2\sqrt{6}}{x^{10/3}} \sum_{k=1}^{\infty} e^{-b_k/x^2} b_k^{2/3} U(-5/6, 4/3, b_k/x^2), \tag{2}$$

where $b_k = 2\alpha_k^3/27$ and $U(a, b, z)$ is the confluent hypergeometric function.[4] The function $f(x)$ has the asymptotic tails,[3,5]

$$f(x) \sim x^{-5} e^{-2\alpha_1^3/27x^2} \quad \text{as} \quad x \to 0$$
$$f(x) \sim e^{-6x^2} \quad \text{as} \quad x \to \infty. \tag{3}$$

A plot of this function, obtained by evaluating the sum in Eq. (2) using the Mathematica, is provided in Fig. 1.

So, why would anyone care about such a complicated function? The reason behind the sustained interest and study[3,5–8] of this function $f(x)$ seems to be the fact that it keeps resurfacing in a number of seemingly unrelated problems, mostly in computer science and graph theory [for a list of such problems see ref. 6]. For example, the function $f(x)$ describes the distribution of the cost of the construction of a linear table for data storage using the linear probing with random hashing algorithm.[6] The function $f(x)$ also describes the distribution of the total path length in Catalan trees.[3] The generating function for the number of inversions in trees involves the Airy distribution function $f(x)$.[9] Also, the moments M_n's of the function $f(x)$ appear in the enumeration of the connected components in a random graph.[10,11] Recently, it has been conjectured and subsequently tested numerically that the asymptotic distribution of the area of two dimensional self-avoiding polygons is also given by the Airy distribution function $f(x)$.[12] Besides, numerical evidence suggests

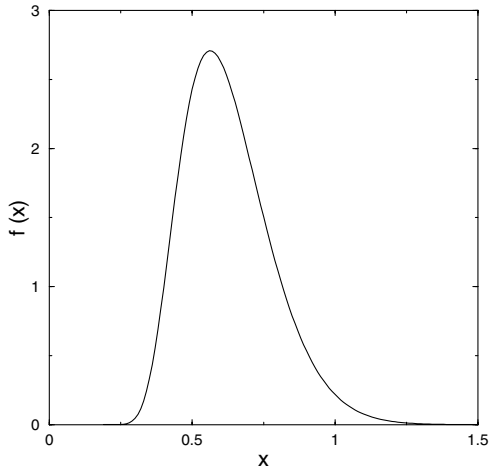

Fig. 1. A Mathematica plot of the Airy distribution function $f(x)$ in Eq. (2).

that the area enclosed by the outer boundary of planar random loops is also distributed according to the Airy distribution function $f(x)$.[13] Given the widespread occurrence of this function $f(x)$ in various combinatorial problems, it is natural to ask whether this function also appears in a more realistic physical system. In a recent Letter,[14] we have demonstrated that indeed this Airy distribution function also appears in a rather well studied physical system, namely the one dimensional fluctuating interfaces.

Fluctuating interfaces have been widely studied over the last two decades as they appear in a variety of physical systems such as growing crystals, molecular beam epitaxy, fluctuating steps on metals and growing bacterial colonies.[15,16] The past theoretical efforts mostly concentrated in characterizing the universal scaling properties of the surface roughness measured via the average width of the surface. This average roughness, however, fails to measure the possible extreme fluctuations which, though rare, may play an important role under many situations. For example, extreme fluctuations play a significant role in batteries where a short circuit may occur if the highest point of the metal surface on one electrode reaches the one on the opposite electrode. There is also a compelling theoretical motivation for studying the extreme fluctuations. While the extreme value statistics is well understood for a set of *independent* random variables,[17] it becomes nontrivial when the random variables are *correlated*. The extreme value problems associated with correlated variables have appeared recently in a variety of problems ranging from disordered systems[18] to a number of computer science problems that include the growing search trees[19] and the networks.[20] A fluctuating interface is an ideal candidate for studying the extreme statistics of correlated variables since the heights at two different points on the interface are correlated. A knowledge of the distribution of their maximum (or minimum) may possibly provide important insights into this important general class of extreme value problems of correlated variables.

Motivated by these observations, Raychaudhury *et al.*[21] recently proposed to study the statistics of the global maximal relative height (MRH) (measured with respect to the spatially averaged growing height) of a fluctuating $(1+1)$-dimensional interface. By $(1+1)$-dimensional interface one means an interface characterized by a scalar height function $H(x,t)$ growing over a linear substrate. For a substrate of finite size L, the system reaches a stationary state in the long time limit. In this stationary state, the MRH h_m is expected to scale as the surface roughness, $h_m \sim L^{\alpha}$ for large L, where α is the roughness exponent. This suggests, quite generically, a scaling form for the normalized probability distribution of the MRH, $P(h_m, L) \sim L^{-\alpha} f_1(h_m/L^{\alpha})$ where $f_1(x)$ is a scaling function. This was demonstrated numerically in ref. 21 for a one dimensional lattice

model belonging to the Edwards–Wilkinson (EW) universality class.[22] Further, it was argued that the scaling function $f_1(x)$ is sensitive to the boundary conditions.[21]

In our previous Letter,[14] using path integral techniques, we presented an exact solution of the stationary MRH distribution $P(h_m, L)$ for the $(1+1)$-dimensional EW model, with both periodic and free boundary conditions. For the periodic case, we showed that $P(h_m, L) = L^{-1/2} f\left(h_m L^{-1/2}\right)$ for all $L > 0$ where the scaling function $f(x)$ is precisely the Airy distribution function defined in Eq. (1). For the free boundary case, the same scaling was found to hold though the scaling function was different from that of the periodic case. The purpose of the present paper is twofold: (i) to provide detailed derivations of various results that were just announced in ref. 14 and (ii) to extend our results to other systems such as the Kardar–Parisi–Zhang (KPZ) interface.[23] Our main results, along with a layout of the paper, are summarized below.

1. In Section 2.1, we provide a new physical derivation, using methods of path integral, of the distribution of the area under a Brownian excursion. This result is used later in Section 4.1 in the context of the MRH distribution of an EW interface with periodic boundary condition. In Section 2.2, we derive the distribution of the area under a Brownian meander (a Brownian meander is a one dimension Brownian motion $x(\tau)$ over the time interval $0 \leqslant \tau \leqslant T$ that is pinned to the origin at one end $x(0) = 0$, but is free at the other end at $\tau = T$, and is constrained to stay positive in between). These results for the Brownian meander will be used later to discuss the MRH distribution of an EW interface with free boundary condition in Section 4.2. The Section 2 can be read independently of the rest of the paper and the results here are interesting by themselves.

2. Section 3 includes a detailed derivation of various correlation functions in the EW model in two opposite regimes: (a) *growing regime* where the correlation length of the interface $\xi(t) \sim t^{1/z}$ (z being the dynamical exponent) is less than the system size, $\xi(t) << L$ and (b) *stationary regime* when $\xi(t) >> L$ and thus the joint probability distribution of height fluctuations become time independent. An explicit form of this joint distribution in the stationary regime is derived for both periodic and free boundary conditions.

3. In Section 4, we derive analytically the stationary MRH distribution in $(1+1)$-dimensional EW model. Section 4.1 discusses the periodic boundary condition case, where the scaled MRH distribution is shown to be exactly the Airy distribution function defined in Eq. (1). The moments of this distribution are also computed exactly. The analytical results are

then compared to the numerical results obtained from the direct numerical integration of the EW equation and an excellent agreement is found. In Section 4.2, we derive the MRH distribution for the EW interface with free boundary condition and show that it is related to the area under two independent Brownian meanders. We call the associated scaling function F-Airy distribution function where F refers to the free boundary condition. We also compute the moments and the asymptotic properties of this distribution analytically. As in the periodic case, we find excellent agreement between the analytical and the numerical results.

4. In Section 5, we discuss the $(1+1)$-dimensional KPZ equation and show that for the periodic boundary condition, the stationary MRH distribution is again given by the Airy distribution function in Eq. (1). This is further confirmed by direct numerical integration of the $(1+1)$-dimensional KPZ equation.

5. Section 6 discusses the MRH distribution in the growing regime $t << L^z$. Using the well known theory of the extreme value statistics of *independent* random variables, we show that the appropriately scaled MRH distribution is universal and is given by the Gumbel function.

6. We conclude in Section 7 with a summary, experimental consequences of our results and some open questions.

2. THE AREA UNDER A BROWNIAN EXCURSION AND A BROWNIAN MEANDER

In this section, we provide a new derivation, using path integral methods, of the distribution of the area under a Brownian excursion and a Brownian meander. These results were originally derived by mathematicians[1–3,24,25] using various probabilistic methods. The path integral method presented here, though perhaps not rigorous in the strict mathematical sense, does provide a simpler physical derivation. Thus the results of this section are interesting by themselves and can be read independently of the rest of the paper that discusses the fluctuating interfaces. This section will also serve as an introduction to the path integral method to be used in later sections to study the maximal height fluctuations in interfaces.

2.1. Brownian Excursion

A Brownian excursion is a one dimensional Brownian motion over the time interval $0 \leqslant \tau \leqslant T$ that starts and ends at the origin $x(0)=x(T)=0$, but is constrained to stay positive in between. We are interested in

computing the probability distribution $P(A,T)$ of the area $A=\int_0^T x(\tau)d\tau$ under the excursion. The Brownian excursion, as described above, is however a bit ill defined for a Brownian walk in continuous space and time. For such a walk, it is well known that if the walker crosses zero once, it recrosses the zero infinitely many times immediately after the first crossing. Thus, for a continuous space–time Brownian motion, it is impossible to enforce the constraint $x(0)=0$ and simultaneously forcing it to stay positive immediately after. There are two ways to go around this problem. The cleanest way to study an excursion is to consider a discrete time random walk moving on a discrete one dimensional lattice and then sample all configurations that start at the origin and come back to the origin for the first time after an even $T=2n$ number of steps. Such paths are called Dyck paths.[3] One then defines the area under such a path as $A=\sum_{i=1}^{2n} x_i$ where x_i is the position of the walker at step i. By appropriately taking the continuum limit, one would then arrive at the Brownian excursion.[26] This method, though conceptually clear, is somewhat cumbersome mathematically.

Here we devise a second method that turns out to be more amenable to path integral techniques. We consider the Brownian motion in continuous space and time, but introduce a small cut-off ϵ by hand as shown in Fig. 2. More precisely, our Brownian motion starts at $x(0)=\epsilon$ and comes back after time T to $x(T)=\epsilon$, without crossing the origin in between. We will first derive the probability density $P(A,T,\epsilon)$ of the area $A=\int_0^T x(\tau)d\tau$ for a fixed ϵ and then finally take the limit $\epsilon\to 0$. We will show that the limiting distribution exists and is precisely the Airy distribution function defined in Eq. (1).

The probability measure associated with an unconstrained Brownian path $x(\tau)$ over the time interval $0\leqslant\tau\leqslant T$ is proportional to $\exp\left[-\frac{1}{2}\int_0^T\left(\frac{dx}{d\tau}\right)^2 d\tau\right]$. In addition, we need to incorporate the constraint that it stays positive between 0 and T which can be achieved by multiplying the above measure with the indicator function $\prod_{\tau=0}^{T}\theta[x(\tau)]$ which is 1 if the path stays positive in $0\leqslant\tau\leqslant T$ and zero otherwise. The distribution $P(A,T)$ of the area $A=\int_0^T x(\tau)d\tau$ under this Brownian excursion can then be expressed as a path integral

$$P(A,T)=\frac{1}{Z_E}\int_{x(0)=\epsilon}^{x(T)=\epsilon}\mathcal{D}x(\tau)\,e^{-\frac{1}{2}\int_0^T d\tau\,(dx/d\tau)^2}\times\prod_{\tau=0}^{T}\theta[x(\tau)]\,\delta\left(\int_0^T x(\tau)d\tau-A\right). \tag{4}$$

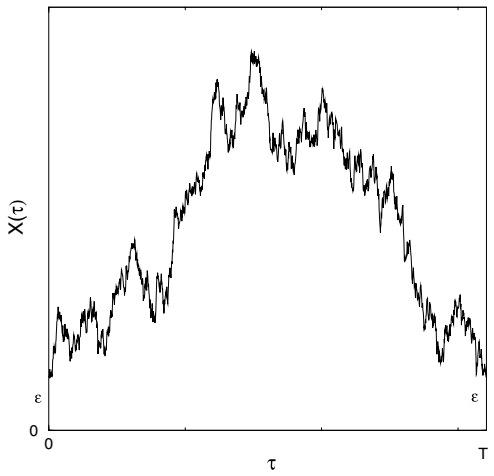

Fig. 2. A Brownian excursion over the time interval $0 \leqslant \tau \leqslant T$ starting at $x(0) = \epsilon$ and ending at $x(T) = \epsilon$ and staying positive in between.

Note that we have suppressed the ϵ dependence of $P(A, T)$ for brevity. The normalization of the distribution, $\int_0^\infty P(A, T) dA = 1$, is ensured by the following definition of the partition function Z_E of the Brownian excursion

$$Z_E = \int_{x(0)=\epsilon}^{x(T)=\epsilon} \mathcal{D}x(\tau)\, e^{-\frac{1}{2}\int_0^T d\tau\, (dx/d\tau)^2} \prod_{\tau=0}^{T} \theta[x(\tau)]. \tag{5}$$

All paths inside the path integrals in Eqs. (4) and (5) propagate from their initial value $x(0) = \epsilon$ at $\tau = 0$ to their final value $x(0) = \epsilon$ at $\tau = T$.

We first evaluate the partition function Z_E. This is easy since one can identify the quantity inside the exponential in Eq. (5) as the action corresponding to a single particle quantum Hamiltonian, $\hat{H}_0 \equiv -\frac{1}{2}\frac{d^2}{dx^2} + V_0(x)$, where the potential $V_0(x) = 0$ for $x > 0$ and $V_0(x) = \infty$ for $x \leqslant 0$. The infinite potential for $x \leqslant 0$ ensures that the path never crosses zero and thus takes care of the indicator function $\prod_{\tau=0}^{T} \theta[x(\tau)]$ in Eq. (5). Using the standard bra–ket notation, the partition function Z_E is then simply the propagator

$$Z_E = \langle \epsilon | e^{-\hat{H}_0 T} | \epsilon \rangle. \tag{6}$$

It is easy to see that the Hamiltonian $\hat{H}_0$ has continuous eigenvalues $E_0 = k^2/2$ labeled by $k \geqslant 0$ and the corresponding eigenfunctions that vanish at

the origin are given by, $\psi_k(x) = \sqrt{\frac{2}{\pi}} \sin(kx)$. Expanding the propagator in the energy eigenbasis, one gets

$$Z_E = \int_0^\infty dk |\psi_k(\epsilon)|^2 e^{-k^2 T/2} = \frac{1}{\sqrt{2\pi T}} \left(1 - e^{-2\epsilon^2/T}\right). \tag{7}$$

Note that Z_E is just the probability that a Brownain motion goes from $x(0) = \epsilon$ to $x(T) = \epsilon$ in time T without crossing the origin, and hence can also be computed by the standard image method which yields the same answer[27] as in Eq. (7).

We now turn to the evalution of $P(A, T)$ in Eq. (4). Taking the Laplace transform, $\tilde{P}(\lambda, T) = \int_0^\infty P(A, T) e^{-\lambda A} dA$ where $\lambda \geqslant 0$, in Eq. (4) gives,

$$\tilde{P}(\lambda, T) = \frac{1}{Z_E} \int_{x(0)=\epsilon}^{x(T)=\epsilon} \mathcal{D}x(\tau)\, e^{-\int_0^T d\tau \left[\frac{1}{2}(dx/d\tau)^2 + \lambda x(\tau)\right]} \prod_{\tau=0}^{T} \theta[x(\tau)]. \tag{8}$$

The numerator in Eq. (8) can then be identified as the propagator $\langle \epsilon | e^{-\hat{H}_1 T} | \epsilon \rangle$, with the Hamiltonian $\hat{H}_1 \equiv -\frac{1}{2}\frac{d^2}{dx^2} + V_1(x)$ where $V_1(x)$ is a triangular potential: $V_1(x) = \lambda x$ for $x > 0$ and $V_1(x) = \infty$ for $x \leqslant 0$. The later condition again takes care of the fact that the paths do not cross zero. The Hamiltonian $\hat{H}_1$ has only bound states and hence discrete eigenvalues. Solving the corresponding Schrödinger equation, one finds that the wavefunction (up to a normalization constant), that vanishes as $x \to \infty$, is simply given by, $\psi_E(x) = Ai\left[(2\lambda)^{1/3}(x - E/\lambda)\right]$, where $Ai(z)$ is the standard Airy function.[4] The condition that the wavefunction should vanish at $x = 0$ determines the discrete eigenvalues, $E_k = \alpha_k \lambda^{2/3} 2^{-1/3}$ for $k = 1, 2, \ldots$, where α_k's are the magnitude of the zeros of $Ai(z)$ on the negative real axis. For example, one has $\alpha_1 = 2.3381\ldots$, $\alpha_2 = 4.0879\ldots$, $\alpha_3 = 5.5205\ldots$ etc. Thus the normalized eigenfunction is given by

$$\psi_k(x) = \frac{Ai\left[(2\lambda)^{1/3} x - \alpha_k\right]}{\sqrt{\int_0^\infty Ai^2\left[(2\lambda)^{1/3} y - \alpha_k\right] dy}}. \tag{9}$$

The integral $\int_0^\infty Ai^2\left[(2\lambda)^{1/3} y - \alpha_k\right] dy = (2\lambda)^{-1/3} \int_{-\alpha_k}^\infty Ai^2(z) dz$ can be further simplified by using the identity, $\int_{-\alpha_k}^\infty Ai^2(z) dz = [Ai'(-\alpha_k)]^2$[28] where $Ai'(z) = dAi(z)/dz$. Expanding the propagator $\langle \epsilon | e^{-\hat{H}_1 T} | \epsilon \rangle$ into the energy

eigenbasis we get

$$\langle \epsilon | e^{-\hat{H}_1 T} | \epsilon \rangle = \sum_{k=1}^{\infty} |\psi_k(\epsilon)|^2 e^{-\lambda^{2/3} 2^{-1/3} \alpha_k T}. \tag{10}$$

Using the exact eigenfunctions from Eq. (9) and then substituting all the expressions in Eq. (8) we get

$$\tilde{P}(\lambda, T) = \frac{(2\lambda)^{1/3} \sqrt{2\pi T}}{\left(1 - e^{-2\epsilon^2/T}\right)} \sum_{k=1}^{\infty} \frac{Ai^2\left[(2\lambda)^{1/3}\epsilon - \alpha_k\right]}{Ai'^2[-\alpha_k]} e^{-\lambda^{2/3} 2^{-1/3} \alpha_k T}. \tag{11}$$

We are now ready to take the $\epsilon \to 0$ limit. Expanding both the numerator and the denominator in Eq. (11) in a Taylor series in ϵ and taking the $\epsilon \to 0$ limit, we get a simplified result,

$$\tilde{P}(\lambda, T) = \sqrt{2\pi}\, (\lambda T^{3/2}) \sum_{k=1}^{\infty} e^{-2^{-1/3} \alpha_k (\lambda T^{3/2})^{2/3}}. \tag{12}$$

Note that the right hand side of Eq. (12) is a function of only one scaling combination $s = \lambda T^{3/2}$. This demands that the distribution $P(A, T)$ must have the scaling form $P(A, T) = T^{-3/2} f\left(A\, T^{-3/2}\right)$, so that its Laplace transform is a function of only the combination $s = \lambda T^{3/2}$, $\tilde{P}(\lambda, T) = \int_0^\infty f(x) e^{-\lambda T^{3/2} x} dx$. Comparing this to the right hand side of Eq. (12) we arrive at the final result

$$\tilde{f}(s) = \int_0^\infty f(x) e^{-sx} dx = s\sqrt{2\pi} \sum_{k=1}^{\infty} e^{-\alpha_k s^{2/3} 2^{-1/3}}. \tag{13}$$

Moments of the area distribution: Using the scaling form, $P(A, T) = T^{-3/2} f\left(A\, T^{-3/2}\right)$, one finds that the moments $A_n = \int_0^\infty A^n P(A, T) dA = M_n T^{3n/2}$, where $M_n = \int_0^\infty f(x)\, x^n dx$ are the moments of the area under the excursion over a unit interval. The extraction of the moments M_n explicitly from the Laplace transform in Eq. (13) is highly nontrivial. However, starting from Eq. (13), Takacs found a recursive method to compute the moments.[3] We summarize the main results here without the details. One first defines a set of new variables K_n via the relation

$$M_n = \sqrt{\pi}\, 2^{(4-n)/2} \frac{\Gamma(n+1)}{\Gamma\left(\frac{3n-1}{2}\right)} K_n, \tag{14}$$

where $\Gamma(x)$ is the Gamma function. The variables K_n's subsequently satisfy a nonlinear recurrence

$$K_n = \frac{3n-4}{4} K_{n-1} + \sum_{j=1}^{n-1} K_j K_{n-j}, \tag{15}$$

starting with $K_0 = -1/2$. This produces recursively the exact values of the moments M_n for any n. For example, the first few values are,

$$M_0 = 1, \quad M_1 = \frac{1}{2}\sqrt{\frac{\pi}{2}}, \quad M_2 = \frac{5}{12}, \quad M_3 = \frac{15}{64}\sqrt{\frac{\pi}{2}}, \quad M_4 = \frac{221}{1008}, \ldots \tag{16}$$

These moments will be used later in Section 4.1 in the context of the maximal height fluctuations in interfaces with periodic boundary conditions.

2.2. Brownian Meander

A Brownian meander is a path of a one dimensional Brownian motion over the time interval $0 \leqslant \tau \leqslant T$ that starts at the origin $x(0) = 0$ and stays positive upto $\tau = T$. The difference between an excursion and a meander is that in the former case, the path comes back to the origin at the end of the interval, $x(T) = 0$. In the case of the meander, the Brownian walker is free to arrive at any final position as long as the final position is positive. As in the case of the Brownian excursion in the previous subsection, we consider the Brownian meander in continuous space and time, but introduce a small cut-off in the initial position $x(0) = \epsilon$, and eventually take the $\epsilon \to 0$ limit. In Fig. 3, we show a Brownian meander that finally arrives at the position $b > 0$ at time $\tau = T$, starting at $x(0) = \epsilon$. Contrary to the Brownian excursion where the final position is same as the initial position i.e., $x(T) = b = \epsilon$, for the meander we need to integrate the paths over all possible final positions $b > 0$.

As before, we are interested in computing the probability distribution $P(A, T)$ of the area $A = \int_0^T x(\tau) d\tau$ under a meander. We suppress the ϵ and b dependence of $P(A, T)$ for brevity. Following the same arguments as in Section 2.1, one can easily write down an expression for the Laplace transform, $\tilde{P}(\lambda, T) = \int_0^\infty P(A, T) e^{-\lambda A} dA$, as a ratio of two propagators,

$$\tilde{P}(\lambda, T) = \frac{\int_0^\infty db \langle b | e^{-\hat{H}_1 T} | \epsilon \rangle}{\int_0^\infty db \langle b | e^{-\hat{H}_0 T} | \epsilon \rangle}, \tag{17}$$

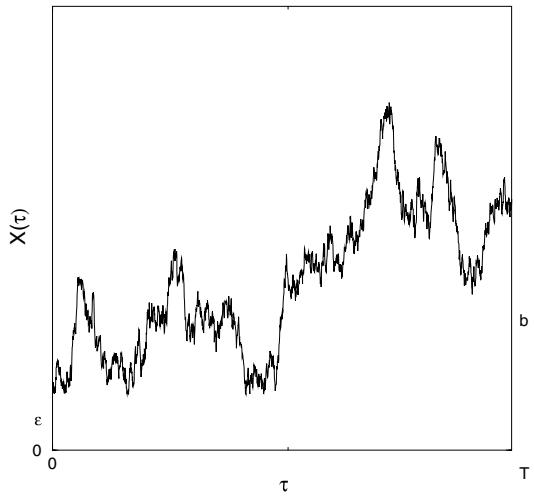

Fig. 3. A Brownian meander over the time interval $0 \leqslant \tau \leqslant T$ starting at $x(0) = \epsilon$ and ending at $x(T) = b$ and staying positive in between.

where the Hamiltonians $\hat{H}_0$ and $\hat{H}_1$ are the same as in the previous subsection.

The denominator, $Z_M = \int_0^\infty db \langle b|e^{-\hat{H}_0 T}|\epsilon\rangle$, is the partition function of the Brownian meander and can be easily evaluated by decomposing the propagator in the energy eigenbasis of $\hat{H}_0$. We get

$$Z_M = \mathrm{erf}(\epsilon/\sqrt{2T}), \tag{18}$$

where $\mathrm{erf}(x) = \frac{2}{\sqrt{\pi}} \int_0^x e^{-u^2} du$ is the standard Error function. Note that Z_M is simply the probability that a Brownian walker does not return to the origin upto time T starting at the initial position ϵ and hence, can be computed also via the method of images.[27]

The propagator in the numerator in Eq. (17) can be evaluated by expanding it in the energy eigenbasis of $\hat{H}_1$, which were detailed in Section 2.1. We do not repeat the calculations here and just mention the final result. We get

$$\tilde{P}(\lambda, T) = \frac{1}{\mathrm{erf}(\epsilon/\sqrt{2T})} \sum_{k=1}^{\infty} \frac{Ai[(2\lambda)^{1/3}\epsilon - \alpha_k] \int_{-\alpha_k}^{\infty} Ai(z) dz}{Ai'^2(-\alpha_k)} e^{-\lambda^{2/3} 2^{-1/3} \alpha_k T}, \tag{19}$$

where α_k's are the magnitude of the zeros of the Airy function. Taking the $\epsilon \to 0$ limit we obtain a simpler expression

$$\tilde{P}(\lambda, T) = \sqrt{\pi}\, 2^{-1/6}\, (\lambda T^{3/2})^{1/3} \sum_{k=1}^{\infty} B(\alpha_k) e^{-2^{-1/3}\alpha_k (\lambda T^{3/2})^{2/3}}, \tag{20}$$

where

$$B(\alpha_k) = \frac{\int_{-\alpha_k}^{\infty} Ai(z)dz}{Ai'(-\alpha_k)}. \tag{21}$$

One should compare this result with its analogue in the case of the Brownian excursion in Eq. (12). As in the case of the excursion, the right hand side of Eq. (20) is a function of only one scaling combination, $s = \lambda T^{3/2}$. This indicates that $P(A, T) = T^{-3/2}\, g\left(A\, T^{-3/2}\right)$, where the Laplace transform of the scaling function $g(x)$ is obtained from Eq. (20),

$$\tilde{g}(s) = \int_0^{\infty} g(x)\, e^{-sx} dx = \sqrt{\pi}\, 2^{-1/6}\, s^{1/3} \sum_{k=1}^{\infty} B(\alpha_k) e^{-\alpha_k s^{2/3} 2^{-1/3}}. \tag{22}$$

To make contact with the existing results in the probability literature, we first note that the Laplace transform, $\tilde{P}(\lambda, T) = \int_0^{\infty} P(A, T) e^{-\lambda A} dA$ can be regarded as the expectation value $E[e^{-\lambda A}]$ with respect to the probability distribution $P(A, T)$. Next, in terms of a new scaling variable $t = 2^{-1/3}\lambda^{2/3} T$, Eq. (20) can be rewritten in a simpler form,

$$E\left[e^{-\sqrt{2}t^{3/2}a}\right] = \sqrt{\pi t} \sum_{k=1}^{\infty} B(\alpha_k) e^{-\alpha_k t}, \tag{23}$$

where we have defined the scaled area $a = A/T^{3/2}$. Note that, as in the case of an excursion, the interval length T only appears as a trivial scale factor and hence one can interpret a as the area under a Brownian meander over the unit interval $[0, 1]$. Dividing both sides of Eq. (23) by $\sqrt{\pi t}$ and taking a further Laplace transform with respect to t, we get

$$\int_0^{\infty} \frac{dt}{\sqrt{\pi t}} e^{-ut} E\left[e^{-\sqrt{2}t^{3/2}a}\right] = \sum_{k=1}^{\infty} \frac{B(\alpha_k)}{(\alpha_k + u)} = \frac{\int_u^{\infty} Ai(z)dz}{Ai(u)}. \tag{24}$$

The second equality in Eq. (24) can be proved by replacing the sum by a contour integration in the complex plane, a derivation of which is given in

Appendix A. This result in Eq. (24) is identical to an expression derived by Perman and Wellner[24] using probabilistic methods. Here we have provided a simpler physical derivation using path integral techniques.

Moments of the area distribution: The scaling form $P(A,T) = T^{-3/2} g\left(A\, T^{-3/2}\right)$ indicates that the moments of the area under a Brownian meander are given as $A_n = \int_0^\infty A^n P(A,T) dA = a_n T^{3n/2}$, where $a_n = \int_0^\infty g(x)\, x^n dx$ are the moments of the area under a Brownian meander over the unit interval. As in the case of Brownian excursion, the extraction of the moments a_n's explicitly from the Laplace transform in Eq. (22) is not easy. However, starting from the alternative expression of the Laplace transform in Eq. (24), Perman and Wellner were able to obtain the moments a_n's recursively.[24] Here we briefly summarize their results without the details. We first define a set of new variables R_n's via the relation

$$a_n = \sqrt{\pi}\, 2^{-n/2} \frac{\Gamma(n+1)}{\Gamma\left(\frac{3n+1}{2}\right)} R_n. \tag{25}$$

Next, the R_n's were found to satisfy the following recursion relations[24] for all $n \geqslant 1$,

$$\begin{aligned} R_n &= \beta_n - \sum_{j=1}^{n} \gamma_j R_{n-j} \\ \beta_n &= \gamma_n + \frac{3}{4}(2n-1)\beta_{n-1} \\ \gamma_n &= \frac{(36)^{-n}}{\Gamma(n+1)} \frac{\Gamma(3n+1/2)}{\Gamma(n+1/2)}. \end{aligned} \tag{26}$$

Using Eqs. (26) and (25), the moments a_n's can be subsequently calculated recursively. The first few values are

$$a_0 = 1, \quad a_1 = \frac{3}{4}\sqrt{\frac{\pi}{2}}, \quad a_2 = \frac{59}{60}, \quad a_3 = \frac{465}{512}\sqrt{\frac{\pi}{2}}, \ldots \tag{27}$$

We will use these results later in the context of the calculation of the moments of the maximal height fluctuations in interfaces with free boundary conditions.

3. FLUCTUATING EW INTERFACE

In this section, we will discuss some general properties of the dynamics and the stationary state of a fluctuating $(1+1)$-dimensional interface. We consider here the simplest model of a fluctuating one dimensional interface characterised by a single valued height function $H(x,t)$ which is growing on a linear substrate of size L according to the celebrated EW equation[22]

$$\frac{\partial H(x,t)}{\partial t} = \frac{\partial^2 H(x,t)}{\partial x^2} + \eta(x,t), \tag{28}$$

where $\eta(x,t)$ is a Gaussian white noise with zero mean and a correlator, $\langle \eta(x,t)\eta(x't')\rangle = 2\delta(x-x')\delta(t-t')$. The Eq. (28) has a soft (zero wave vector) mode since the spatially averaged height $\overline{H(x,t)} = \int_0^L H(x,t)dx/L$ diffuses with time (typical value growing as $\sqrt{t/L}$) even in a finite system of size L. Thus, the joint height distribution $P[\{H\},t]$ of the system will never reach a time independent stationary state. Hence, it is useful to subtract this zero mode from the height and define the relative height, $h(x,t) = H(x,t) - \overline{H(x,t)}$, whose joint distribution $P[\{h\},t]$ will eventually reach a stationary state in the long time limit in a finite system. Note that the average height $\overline{H(x,t)}$ is over a given sample, and not the statistical average over the noise η in Eq. (28). So, from now on, we will always consider the relative height $h(x,t)$ as our basic variables. Note that, by definition,

$$\int_0^L h(x,t)dx = 0. \tag{29}$$

We will see later that this constraint of zero total area under the relative height h plays an important role in determining the MRH distribution. All the other nonzero modes of h evolve identically as those of the actual height H.

We will see shortly that there are two regimes of the evolution of the interface in a finite system. Let us assume that we start from a flat initial configuration where the heights at different points on the substrate are completely uncorrelated from each other. As time t grows, the heights at different points get correlated and the system is characterized by a single growing correlation length $\xi(t) \sim t^{1/z}$, where z is the dynamical exponent ($z=2$ for the EW interface). As long as this growing correlation length is much smaller than the system size, $\xi(t) \sim t^{1/z} << L$, the interface is in the *growing regime*. In this regime, the system does not feel the boundary

and hence is insensitive to the boundary conditions. When the correlation length becomes comparable or exceeds the system size, $\xi(t) \sim t^{1/z} \geqslant L$, the system crosses over to a *stationary regime* where the joint distribution of relative heights $P[\{h\}, t]$ becomes time independent. In this regime, the system is strongly sensitive to the boundary conditions. The crossover time between the two regimes scales as $t_c \sim L^z$.

The two subsections below deal with two different boundary conditions, respectively the periodic and the free boundary condition. Our goal in these subsections would be to compute the height–height correlation function as well as the stationary joint distribution of the relative heights $P[\{h\}]$ for the two boundary conditions. The form of these joint distributions will be used later in Section 4 for the calculation of the MRH distribution in the stationary state.

3.1. Periodic Boundary Conditions

We first consider the periodic boundary condition, $H(0,t) = H(L,t)$. The relative height $h(x,t) = H(x,t) - \int_0^L H(x,t)dx/L$ satisfies the same boundary condition, $h(0,t) = h(L,t)$ and also satisfies the same evolution Eq. (28) as the actual height $H(x,t)$. Since the relative height $h(x,t)$ is a periodic function, one can decompose it into a Fourier series, $h(x,t) = \sum_{m=-\infty}^{\infty} \tilde{h}(m,t) e^{2\pi i m x/L}$. Substituting this in Eq. (28), one finds that different nonzero Fourier modes decouple from each other and one can easily calculate any correlation function. For example, the height–height correlation function is given by the exact expression,

$$C(x = |x_1 - x_2|, t, L) = \langle h(x_1,t) h(x_2,t) \rangle = \frac{L}{4\pi^2} \sum_{m \neq 0} \frac{1}{m^2} \left[1 - e^{-8\pi^2 m^2 t/L^2} \right] e^{2\pi i m (x_1 - x_2)/L}, \tag{30}$$

where the sum ranges from $m = -\infty$ to $m = \infty$ excluding the $m = 0$ term.

In the *growing regime* when $t << L^2$, we can make a change of variable $k = 2\pi m \sqrt{t}/L$. Since $t << L^2$, $dk = 2\pi\sqrt{t}/L$ is small and hence k can be considered as a continuous variable. One can then replace the sum in Eq. (30) by an integral over the k space. This integral can be easily performed and one gets,

$$C(x,t) = \sqrt{t}\, G\left(x/\sqrt{t} \right), \tag{31}$$

with the scaling function, $G(y) = \sqrt{\frac{2}{\pi}} e^{-y^2/8} - \frac{1}{2} y \operatorname{erfc}\left(y/\sqrt{8}\right)$, where $\operatorname{erfc}(x) = \frac{2}{\sqrt{\pi}} \int_x^\infty e^{-u^2} du$ is the complementary Error function. The scaling function $G(y)$ starts at $G(0) = \sqrt{2/\pi}$ and decays for large y as $G(y) \approx \frac{4\sqrt{2}}{\sqrt{\pi} y^2} e^{-y^2/8}$. The onsite variance grows as , $\langle h^2(0) \rangle = C(0,t) \sim t^{1/2}$ indicating that the typical relative height in this regime grows as a power law, $h \sim t^\beta$ where the growth exponent $\beta = 1/4$ for the $(1+1)$-dimensional EW interface. The height–height correlation between two sites, at a finite time $t << L^2$ and separated by a large distance $1 << x << L$, decays as $C(x,t) \approx \frac{4\sqrt{2} t^{3/2}}{\sqrt{\pi} x^2} e^{-x^2/8t}$. Thus, in this growing regime, the correlations decay over a length scale $\xi(t) \sim t^{1/2} << L$ which is much smaller than the system size L.

In the opposite *stationary regime* when $t >> L^2$, one can drop the exponential factor in Eq. (30). The correlation function becomes time independent. Summing the resulting series in Eq. (30) one gets,

$$C(x, L) = \frac{L}{12} \left[1 - \frac{6x}{L} \left(1 - \frac{x}{L} \right) \right]. \tag{32}$$

Thus, the onsite variance $\langle h^2(0) \rangle = C(0, L) = L/12$. It is evident from Eq. (32) that in the *stationary regime*, the heights at different space points are *strongly* correlated. In Section 5, we will calculate exactly the distribution of the maximum of these heights in the stationary regime. Thus, our result will provide an exact solution of the distribution of the extremum of a set of strongly correlated random variables.

We are now ready to write down the joint distribution of heights $P[\{h\}]$ in the stationary state. For simplicity, let us first consider the single site stationary height distribution $P(h, t \to \infty)$. Because of the linearity of Eq. (28) the stationary measure on h is Gaussian. Using $\langle h^2(0) \rangle = C(0, L) = L/12$, the stationary single site height distribution is Gaussian,

$$P_{\rm st}(h) = \sqrt{\frac{6}{\pi L}} e^{-6h^2/L}. \tag{33}$$

Moreover, from Eq. (30), one can easily show that the slope–slope correlation function, $\langle \partial_x h \partial_{x'} h \rangle \to \delta(x - x') - 1/L$ in the stationary state. The local slopes $\partial_x h$ are thus uncorrelated in the stationary state, except for the overall constraint due to the periodic boundary condition, $\int_0^L dx\, \partial_x h = 0$, that gives rise to the residual $1/L$ term. Collecting these facts together and remembering the constraint in Eq. (29), one readily writes down the

stationary joint distribution of heights (a multivariate Gaussian distribution),

$$P[\{h\}] = A_L\, e^{-\frac{1}{2}\int_0^L d\tau (\partial_\tau h)^2}\, \delta[h(0) - h(L)]\, \delta\left[\int_0^L h(\tau) d\tau\right], \tag{34}$$

where A_L is a normalization constant and the two delta functions take care respectively of the periodic boundary condition $h(0) = h(L)$ and the zero area constraint in Eq. (29). Note that in Eq. (34), τ refers to the space (and not time) and varies over the interval $0 \leqslant \tau \leqslant L$. In fact, from now on we will use τ to denote the space in order to make correspondence with the results derived in Section 2.

Before proceeding to calculate the normalization constant A_L, we make one important remark here. The exponential factor inside the probability measure in Eq. (34) indicates that the stationary paths are locally Brownian, i.e., evolve in space as, $dh(\tau)/d\tau = \xi(\tau)$, where $\xi(\tau)$ is a Gaussian white noise with zero mean and a correlator, $\langle \xi(\tau)\xi(\tau')\rangle = \delta(\tau - \tau')$. For the periodic boundary condition, the stationary path in space is, in fact, a Brownian bridge. This stationary Brownian measure also follows rather obviously even from the basic EW equation in Eq. (28) whose equilibrium Gibbs–Bolzmann state precisely corresponds to the exponential factor in Eq. (34). However, one has to be a bit more careful. The multiplicative factor representing the zero mode constraint, $\delta\left[\int_0^L h(\tau) d\tau\right]$, in Eq. (34) indicates that *only those Brownian bridges should be sampled which enclose a total zero area over the interval* $[0, L]$. Normally, in writing down the stationary measure for the relative heights, one ignores this multiplicative delta function factor simply due to the fact that in most of the calculations on the interfaces, such as in the calculation of the distribution of the stationary width,[29] this constraint does not play any important role. However, as we will see later in Section 4, this constraint does indeed play a major role in determining the *maximal* height distribution in the stationary state. Hence, it is worth being careful in writing the full exact stationary joint distribution of the relative heights keeping all the factors explicitly as done in Eq. (34).

The normalization constant A_L: To determine the normalization constant, we note that if one integrates over the heights at all the intermediate points in Eq. (34) but keeping the heights at the two ends fixed at, say, $h(0) = h(L) = u$, one should recover the stationary single point height distribution $P_{\rm st}(h_0 = u)$ in Eq. (33), i.e.,

$$A_L \int_{h(0)=u}^{h(L)=u} \mathcal{D}h(\tau)\, e^{-\frac{1}{2}\int_0^L d\tau (\partial_\tau h)^2}\, \delta\left[\int_0^L h(\tau) d\tau\right] = \sqrt{\frac{6}{\pi L}} e^{-6u^2/L}. \tag{35}$$

To evaluate the path integral on the left hand side of Eq. (35), we use a simple and elegant method by identifying the path integral as the propagator of a random acceleration process that has been well studied.[30] To make the connection between the two problems, we first note that in the stationary state, the height $h(\tau)$ locally evolves in space as a Brownian motion, $dh(\tau)/d\tau = \xi(\tau)$ where $\xi(\tau)$ is a Gaussian white noise with zero mean and a correlator, $\langle \xi(\tau)\xi(\tau')\rangle = \delta(\tau - \tau')$. But, as mentioned earlier, this by itself is not enough since it does not take into account the important delta function constraint $\delta\left[\int_0^L h(\tau)d\tau\right]$. To incorporate this special condition, let us define a new variable, $X(\tau) = \int_0^\tau h(\tau)d\tau$. The variable $X(\tau)$ then evolves as, $d^2X/d\tau^2 = dh/d\tau = \xi(\tau)$ and hence can be identified as the position of a particle which is randomly accelerated. Thus, to take into account the full probability measure in Eq. (34), one has to consider the joint evolution, in space, of both the variables $[X(\tau), h(\tau)]$ where $X(\tau)$ is the position and the $h(\tau) = dX/d\tau$ is the velocity of the random accelerator. The joint propagator of this random acceleration process $G[X, h, T|X_0, h_0, 0]$, i.e., the probability that the process reaches its final value $[X, h]$ in time T starting from its initial value $[X_0, h_0]$ at time 0, can be easily calculated and is well known[30]

$$G[X, h, T|X_0, h_0, 0] = \frac{\sqrt{3}}{\pi T^2} \exp\left[-\frac{6}{T^3}(X - X_0 - h_0 T)(X - X_0 - hT) - \frac{2}{T}(h - h_0)^2\right]. \tag{36}$$

The next step is to note that the path integral on the left hand side of Eq. (35) is just the propagator of the random acceleration problem in Eq. (36), going from its initial value $[X_0 = 0, h_0 = u]$ to its final value $[X = 0, h = u]$ in 'time' L and hence is given by,

$$\int_{h(0)=u}^{h(L)=u} \mathcal{D}h(\tau)\, e^{-\frac{1}{2}\int_0^L d\tau (\partial_\tau h)^2}\, \delta\left[\int_0^L h(\tau)d\tau\right] = G[0, u, L|0, u, 0] = \frac{\sqrt{3}}{\pi L^2} \exp\left[-6u^2/L\right]. \tag{37}$$

Substituting this result in Eq. (35) and cancelling out the exponential factors from both sides, one gets

$$A_L = \sqrt{2\pi}\, L^{3/2}. \tag{38}$$

3.2. Free Boundary Conditions

In this subsection, we consider the free boundary condition where the slopes of the interface vanish at the two ends, $\partial_x h = 0$ at $x = 0$ and $x = L$. This boundary condition arises naturally if one considers a spatially discretized version of the continuum EW equation,

$$\frac{dh(i,t)}{dt} = h(i+1,t) + h(i-1,t) - 2h(i,t) + \eta(i,t), \tag{39}$$

where $i = 1, 2, \ldots, L$ and $h(i,t)$ can be interpreted as the displacement of the i-th bead of a polymer chain where the beads are connected via harmonic springs, such as in the Rouse model.[31] If the chain forms a cycle, one has the periodic boundary condition. On the other hand, if the two ends of the chain are free, the beads at the two end points feel only one sided interactions, i.e.,

$$\begin{aligned} \frac{dh(L,t)}{dt} &= h(L-1,t) - h(L,t) + \eta(L,t), \\ \frac{dh(1,t)}{dt} &= h(2,t) - h(1,t) + \eta(1,t). \end{aligned} \tag{40}$$

The end point Eq. (40) will be consistent with Eq. (39) provided one incorporates the boundary conditions, $h(L,t) = h(L+1,t)$ and $h(1,t) = h(0,t)$. In the continuum space, this boundary condition is equivalent to having $\partial_x h = 0$ at $x = 0$ and $x = L$.

The zero slope conditions at the two end points indicate that one should decompose the height variable into a cosine series, $h(x,t) = \sum_{m=1}^{\infty} \tilde{h}(m,t) \cos(m\pi x/L)$. As in the periodic case, the different modes evolve independently and one can easily calculate the height–height correlation function. We find,

$$\begin{aligned} C(x_1, x_2, t, L) &= \langle h(x_1,t) h(x_2,t) \rangle \\ &= \frac{2L}{\pi^2} \sum_{m=1}^{\infty} \frac{1}{m^2} \left[1 - e^{-2m^2\pi^2 t/L^2} \right] \cos\left(\frac{m\pi x_1}{L}\right) \cos\left(\frac{m\pi x_2}{L}\right). \end{aligned} \tag{41}$$

Note that, unlike the periodic case in Eq. (30), the correlation function $C(x_1, x_2, t, L)$ is not translationally invariant and depends on both co-ordinates x_1 and x_2.

In the *growing regime* when $t << L^2$, one can again replace the sum in Eq. (41) by an integral over the $k = \pi m \sqrt{t}/L$ variable. The resulting integral can be easily performed and one finds,

$$C(x_1, x_2, t) = \sqrt{t} \left[G\left(\frac{|x_1 - x_2|}{\sqrt{t}} \right) + G\left(\frac{|x_1 + x_2|}{\sqrt{t}} \right) \right] \tag{42}$$

with the same scaling function, $G(y) = \sqrt{\frac{2}{\pi}} e^{-y^2/8} - \frac{1}{2} y \operatorname{erfc}\left(y/\sqrt{8} \right)$, as in the periodic case. Note that in the limit when both x_1 and x_2 are large (but both small compared to L) with the distance between them $x = |x_1 - x_2|$ fixed, Eq. (42) reduces to the same correlation function as in the periodic case in Eq. (31). This is physically expected, since in the growing regime $t << L^2$, the system is insensitive to the boundary conditions.

In the *stationary regime* when $t >> L^2$, the time independent correlation function can be obtained by dropping the exponential factor in Eq. (41) and summing the resulting series. We get,

$$C(x_1, x_2, L) = L \left[\frac{1}{3} - \frac{1}{2L} (x_1 + x_2 + |x_1 - x_2|) + \frac{1}{2L^2} \left(x_1^2 + x_2^2 \right) \right]. \tag{43}$$

In particular, the onsite variance, $\langle h^2(x) \rangle = C(x, x, L) = L \left[\frac{1}{3} - \frac{x}{L} \left(1 - \frac{x}{L} \right) \right]$ now depends on the site co-ordinate x since the translational invariance is lost with free boundary conditions. Note that, as in the periodic case, the heights are *strongly* correlated in the stationary state.

The stationary single point height distribution is Gaussian, $P_{\rm st}(h(x)) = e^{-h^2(x)/2C(x,x,L)}/\sqrt{2\pi C(x, x, L)}$. In particular, the stationary height distribution at $x = 0$ is given by

$$P_{\rm st}(h(0)) = \sqrt{\frac{3}{2\pi L}}\, e^{-3h^2(0)/2L}. \tag{44}$$

One can also calculate the slope–slope correlation function from Eq. (41) and one finds that for $t >> L^2$, $\langle \partial_x h \partial_{x'} h \rangle \to \delta(x - x')$, implying that the slopes get completely uncorrelated in the stationary state. Once again, collecting these facts together and taking into account the constraint in Eq. (29), one finds that the stationary joint distribution of heights for the free boundary case, for fixed boundary heights $h(0) = u$ and $h(L) = v$, is given by

$$P[\{h\}, u, v] = B_L\, e^{-\frac{1}{2}\int_0^L d\tau (\partial_\tau h)^2}\, \delta\left[\int_0^L h(\tau) d\tau \right] \delta[h(0) - u]\, \delta[h(L) - v], \tag{45}$$

where the normalization constant B_L is yet to be determined.

The normalization constant B_L: The constant B_L is calculated using the similar method as in the periodic case. First, we integrate over the heights at all the intermediate points in Eq. (45) but keeping the heights at the two ends fixed, say $h(0)=u$ and $h(L)=v$. This gives us the joint stationary distribution of heights at the two end points, $P_{\rm st}[u, v]$. If we now further integrate over v, we should get the single point height distribution $P_{\rm st}[h(0)=u]$ given in Eq. (44). Thus we have,

$$B_L \int_{-\infty}^{\infty} dv \int_{h(0)=u}^{h(L)=v} \mathcal{D}h(\tau)\, e^{-\frac{1}{2}\int_0^L d\tau (\partial_\tau h)^2}\, \delta\left[\int_0^L h(\tau) d\tau\right] = \sqrt{\frac{3}{2\pi L}} e^{-3u^2/2L}. \tag{46}$$

As in the periodic case, we now identify the path integral on the left hand side of Eq. (46) as the propagator $G[0, v, L|0, u, 0]$ of the random acceleration process in Eq. (36) going from the initial point $[0, u]$ to the final point $[0, v]$ in 'time' L. This gives,

$$\int_{h(0)=u}^{h(L)=v} \mathcal{D}h(\tau)\, e^{-\frac{1}{2}\int_0^L d\tau (\partial_\tau h)^2}\, \delta\left[\int_0^L h(\tau) d\tau\right] = G[0, v, L|0, u, 0] = \frac{\sqrt{3}}{\pi L^2} \exp\left[-\frac{6}{L}uv - \frac{2}{L}(u-v)^2\right]. \tag{47}$$

We substitute this expression of the path integral on the left hand side of Eq. (46) and then integrate over v. Cancelling the exponential factors from both sides of Eq. (46) gives

$$B_L = L. \tag{48}$$

4. MRH DISTRIBUTION IN THE STATIONARY REGIME: EW INTERFACE

In this section, we derive the principal new results of this paper, namely the exact probability distribution of the MRH in the stationary state of the EW equation in a finite one dimensional system of size L, both for periodic and free boundary conditions.

4.1. Periodic Boundary Conditions

Consider the EW model in Eq. (28) in the stationary regime when $t >> L^2$. The exact form of the stationary joint distribution of the relative heights $P[\{h\}]$ is given in Eq. (34) with the normalization constant, $A_L = \sqrt{2\pi}\, L^{3/2}$. We wish to compute the probability distribution of the MRH, $\max[\{h\}]$. Let us first define the cumulative distribution of the MRH, $F(h_m, L) = \text{Prob}[\max\{h\} < h_m, L]$. The distribution of the MRH is simply the derivative, $P(h_m, L) = \partial F(h_m, L)/\partial h_m$. Clearly $F(h_m, L)$ is also the probability that the heights at all points in $[0, L]$ are less than h_m and hence can be written using the measure in Eq. (34) as a path integral,

$$F(h_m, L) = A_L \int_{-\infty}^{h_m} du \int_{h(0)=u}^{h(L)=u} \mathcal{D}h(\tau)\, e^{-\frac{1}{2}\int_0^L d\tau (\partial_\tau h)^2}\, \delta\left[\int_0^L h(\tau) d\tau\right] I(h_m, L), \tag{49}$$

where $I(h_m, L) = \prod_{\tau=0}^{L} \theta(h_m - h(\tau))$ is an indicator function which is 1 if all the heights are less than h_m and zero otherwise. Due to the periodic boundary condition, $h(0) = h(L)$, all the paths inside the path integral propagate from their initial value $h(0) = u$ to their final value $h(L) = u$. Note also that one needs to integrate over the boundary value $h(0) = h(L) = u$ over the allowed range $-\infty \leqslant u \leqslant h_m$. The upper bound $u \leqslant h_m$ follows from the fact that, by definition, h_m is the maximum over all heights in $[0, L]$ including the two end points.

The next crucial step is to make a change of variables, $x(\tau) = h_m - h(\tau)$ and $u' = h_m - u$ in the path integral in Eq. (49) which gives,

$$F(h_m, L) = A_L \int_0^{\infty} du' \int_{x(0)=u'}^{x(L)=u'} \mathcal{D}x(\tau)\, e^{-\frac{1}{2}\int_0^L d\tau (\partial_\tau x)^2}\, \delta\left[\int_0^L x(\tau) d\tau - A\right] I(L), \tag{50}$$

where $I(L) = \prod_{\tau=0}^{L} \theta(x(\tau))$ and $A = h_m L$. Physically, this change of variable just means that we are now measuring the interface height relative to the maximum and denoting it by $-x(\tau)$. The maximal height now corresponds to the level $x = 0$. Note that h_m appears only through the quantity A in the delta function, and hence $F(h_m, L) = \mathcal{F}(A, L)$. In the subsequent analysis, we will keep a general A in Eq. (50) and will substitute $A = h_m L$ only in the final formula.

We already start seeing the formal similarity between Eq. (50) and Eq. (8) in Section 2 for the distribution of area under a Brownian excursion. To be more precise, we take the Laplace transform with respect to A in Eq. (50) which gives,

$$\int_0^\infty \mathcal{F}(A, L) e^{-\lambda A} dA = A_L \int_0^\infty du' < u' | e^{-\hat{H}_1 L} | u' > = A_L \, \mathrm{Tr} \left[e^{-\hat{H}_1 L} \right], \tag{51}$$

where Tr is the trace and $\hat{H}_1$ is precisely the same Hamiltonian that appeared in Section 2 namely, $\hat{H}_1 \equiv -\frac{1}{2}\frac{d^2}{dx^2} + V_1(x)$ where $V_1(x)$ is a triangular potential: $V_1(x) = \lambda x$ for $x > 0$ and $V_1(x) = \infty$ for $x \leqslant 0$. The Hamiltonian $\hat{H}_1$ has only discrete eigenvalues that were obtained in Section 2, $E_k = \alpha_k \lambda^{2/3} 2^{-1/3}$ for $k = 1, 2, \ldots$, where α_k's are the magnitude of the zeros of $Ai(z)$ on the negative real axis. The trace in Eq. (51) can be easily evaluated knowing these eigenvalues and one gets using $A_L = \sqrt{2\pi}\, L^{3/2}$,

$$\int_0^\infty \mathcal{F}(A, L) e^{-\lambda A} dA = \sqrt{2\pi}\, L^{3/2} \sum_{k=1}^{\infty} e^{-\alpha_k \lambda^{2/3} 2^{-1/3} L}. \tag{52}$$

Next we invert the Laplace transform in Eq. (52) using Bromwitch formula and substituting $A = h_m L$ we get the cumulative MRH distribution,

$$F(h_m, L) = \sqrt{2\pi} L^{3/2} \int_{\lambda_0 - i\infty}^{\lambda_0 + i\infty} \frac{d\lambda}{2\pi i} e^{\lambda h_m L} \sum_{k=1}^{\infty} e^{-\alpha_k \lambda^{2/3} 2^{-1/3} L}, \tag{53}$$

where the integration is along any imaginary axis whose real part λ_0 must be to the right of all singularities of the integrand. Taking derivative with respect to h_m in Eq. (53) and making a change of variable, $\lambda = s L^{-3/2}$, we arrive at our main result, $P(h_m, L) = L^{-1/2} f\left(h_m L^{-1/2}\right)$ for all L, where the Laplace transform of $f(x)$ is given by

$$\int_0^\infty f(x) e^{-sx} dx = s\sqrt{2\pi} \sum_{k=1}^{\infty} e^{-\alpha_k s^{2/3} 2^{-1/3}}. \tag{54}$$

Comparing with Eq. (13) in Section 2, we identify the scaling function $f(x)$ as the Airy distribution function that characterizes the probability distribution of the area a under a Brownian excursion over a unit interval.

Thus, the main result of this subsection has been to establish an equivalence in law between two rather different objects: (i) the scaled

MRH $h_m/\sqrt{L}$ in the stationary state of the EW equation (28) over a linear substrate of size L and (ii) the area a under a Brownian excursion over the unit time interval [0, 1],

$$\frac{h_m}{\sqrt{L}} \equiv a, \tag{55}$$

where $\equiv$ means that the object on the left hand side has the same probability distribution as the object on its right hand side.

Moments of the MRH: Using the scaling form, $P(h_m, L) = L^{-1/2} f\left(h_m L^{-1/2}\right)$ for all L, we get $\langle h_m^n \rangle = M_n L^{n/2}$ where $M_n = \int_0^\infty f(x) x^n dx$ are the moments of the Airy distribution function that were computed in Eq. (16) of Section II. In the context of the MRH, only the second moment $\langle h_m^2 \rangle = 5L/12$ was computed previously in ref. 21 by using a different method. Here, we can compute all the moments of MRH recursively.

Asymptotic tails of the MRH distribution: In order to determine the asymptotic behaviors of the MRH distribution, $P(h_m, L) = L^{-1/2} f\left(h_m L^{-1/2}\right)$, we need to know the tails of the function $f(x)$. As mentioned in the introduction, Takacs was able to formally invert the Laplace transform in Eq. (1) and obtained an expression of $f(x)$ in terms of confluent hypergeometric functions as given in Eq. (2). It is easy to obtain the small x behavior of $f(x)$ from Eq. (2), since only the $k=1$ term dominates the sum near $x \to 0$. Using $U(a, b, z) \sim z^{-a}$ for large z,[4] we get as $x \to 0$,

$$f(x) \to \frac{8}{81} \alpha_1^{9/2} x^{-5} \exp\left[-\frac{2\alpha_1^3}{27x^2}\right], \tag{56}$$

where $\alpha_1 = 2.3381074\ldots$. In the context of the MRH distribution, this essential singular tail of the scaling function near $x \to 0$ was conjectured in ref. 21 based on numerics, though the exact form was missing. The asymptotic behavior at large x is more tricky to derive[5] from Eq. (2). However, it is possible to guess the leading behavior of $f(x)$ for large x by examining the behavior of moments M_n. Using the recursion relations for the moments M_n in Section 2 (Eq. (15)), one finds that for large n, $M_n \sim (n/12e)^{n/2}$. Substituting an anticipated large x decay of the form, $f(x) \sim \exp[-ax^b]$ in $M_n = \int_0^\infty f(x) x^n dx$, we get $M_n \sim (n/abe)^{n/b}$ for large n. Comparing this with the exact large n behavior of M_n we get $a=6$ and $b=2$, indicating a Gaussian tail as $x \to \infty$,

$$f(x) \sim e^{-6x^2}. \tag{57}$$

However, we are not able to determine the amplitude (or the next subleading correction) of this Gaussian tail.

Comparison with numerical simulations: Finally, we would like to compare our exact result for the MRH distribution, $P(h_m, L) = L^{-1/2} f\left(h_m L^{-1/2}\right)$ with $f(x)$ given in Eq. (2), to the results of numerical simulations. We numerically integrated the space–time discretized form of Eq. (28),

$$H(i, t+\Delta t) - H(i,t) = \Delta t\,[H(i+1,t) + H(i-1,t) - 2H(i,t)] + \eta_i(t)\sqrt{2\Delta t}, \tag{58}$$

where $\eta_i(t)$'s are independent and identically distributed random variables for each i and t and each drawn from a Gaussian distribution with zero mean and unit variance. We used periodic boundary condition, i.e., $H(0,t) = H(L,t)$ and $H(L+1,t) = H(1,t)$. We chose the time step $\Delta t = 0.01$, and we checked that the results were stable. We used different system sizes $L = 256$, $L = 384$, and $L = 512$. We first evolved Eq. (58) for a long time (typically 2×10^6 Monte Carlo time steps) and ensured that the system has reached the stationary state. After that, the system was further evolved and the data for the histogram of the MRH was sampled at times which are far apart from each other to avoid correlations between them. The number of samples used were typically 2×10^6. In Fig. 4, we have plotted the numerical scaling function generated by collapsing the data for the three system sizes and also plotted the Airy distribution function $f(x)$ by evaluating the sum in Eq. (2) using the Mathematica. The agreement between the analytical and the numerical scaling function is very good.

4.2. Free Boundary Conditions

In this subsection we compute the stationary MRH distribution of the EW equation (28) with free boundary conditions, $\partial_x h = 0$ at $x = 0$ and $x = L$. The stationary joint distribution of relative heights $P[\{h\}, u, v]$ (with boundary heights fixed at $h(0) = u$ and $h(L) = v$) is given in Eq. (45) with $B_L = L$. As in the periodic case, we define the cumulative MRH distribution, $F(h_m, L) = \text{Prob}\,[\max\{h\} < h_m, L]$. Since $F(h_m, L)$ is also the probability that the heights at all points in $[0, L]$ are less than h_m, one can use Eq. (45) to write

$$F(h_m, L) = L \int_{-\infty}^{h_m} du \int_{-\infty}^{h_m} dv \int_{h(0)=u}^{h(L)=v} \mathcal{D}h(\tau)\, e^{-\frac{1}{2}\int_0^L d\tau (\partial_\tau h)^2}\, \delta\left[\int_0^L h(\tau) d\tau\right] I(h_m, L), \tag{59}$$

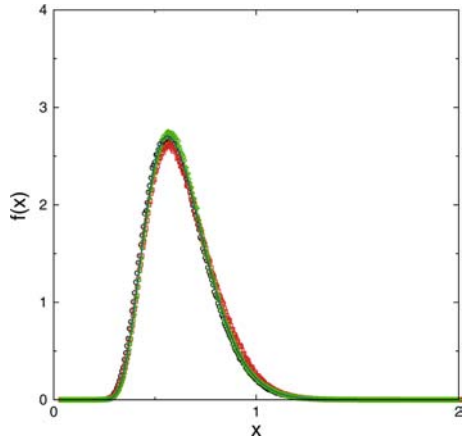

Fig. 4. The scaling function $f(x)$ associated with the MRH distribution , $P(h_m, L) = L^{-1/2} f(h_m/\sqrt{L})$ for the EW equation with periodic boundary condition. The numerical curves (shown by symbols) are obtained by collapsing the data obtained from the numerical integration of Eq. (58) for three system sizes $L = 256$ (circles), $L = 384$ (squares), and $L = 512$ (diamonds). Also plotted is the Mathematica generated analytical scaling function in Eq. (2) as shown by the solid line.

where $I(h_m, L) = \prod_{\tau=0}^{L} \theta(h_m - h(\tau))$, as before, is an indicator function which is 1 if all the heights are less than h_m and zero otherwise. Note that the boundary heights u and v are integrated over their common allowed range $[-\infty, h_m]$.

The next step is to make the change of variables, $x(\tau) = h_m - h(\tau)$, $u' = h_m - u$ and $v' = h_m - v$ where $-x(\tau)$ now denotes the interface height measured relative to the maximal height. The maximal height now corresponds to the level $x = 0$. With these change of variables, Eq. (59) now reads

$$F(h_m, L) = L \int_0^\infty du' \int_0^\infty dv' \int_{x(0)=u'}^{x(L)=v'} \mathcal{D}x(\tau) e^{-\frac{1}{2}\int_0^L d\tau (\partial_\tau x)^2} \delta\left[\int_0^L x(\tau) d\tau - A\right] I(L), \tag{60}$$

where $I(L) = \prod_{\tau=0}^{L} \theta(x(\tau))$ and $A = h_m L$. The only dependence on h_m in Eq. (60) appears through the quantity $A = h_m L$. Hence, $F(h_m, L) = \mathcal{F}(A, L)$. Taking Laplace transform with respect to A in Eq. (60) gives,

$$\int_0^\infty \mathcal{F}(A, L) e^{-\lambda A} dA = L \int_0^\infty du' \int_0^\infty dv' \langle u' | e^{-\hat{H}_1 L} | v' \rangle, \tag{61}$$

where the Hamiltonian $\hat{H}_1$ is the same as in the periodic case. Eq. (61) for the free boundary case should be compared to the corresponding result for the periodic case in Eq. (51) where the integral over the common end points became a trace due to the periodic boundary condition. In the present case, we do not have a trace and evaluating the integral in Eq. (61) would require the knowledge of both the eigenfunctions and the eigenvalues of $\hat{H}_1$. Fortunately, the eigenfunctions can be determined exactly in terms of the Airy function as explained in Section 2. Expanding the propagator $<u'|e^{-\hat{H}_1 L}|v'>$ in Eq. (61) in the energy eigenbasis of $\hat{H}_1$ and using the exact eigenvalues $E_k = \alpha_k \lambda^{2/3} 2^{-1/3}$ for $k = 1, 2, \ldots$ (α_k's being the magnitude of the zeros of $Ai(z)$ on the negative real axis) we get,

$$\int_0^\infty \mathcal{F}(A, L) e^{-\lambda A} dA = L \sum_{k=1}^{\infty} e^{-\alpha_k \lambda^{2/3} 2^{-1/3} L} \int_0^\infty \psi_k(u') du' \int_0^\infty \psi_k(v') dv'. \tag{62}$$

Substituting the exact form of the eigenfunctions $\psi_k(x)$ from Eq. (9) and simplifying, we get

$$\int_0^\infty \mathcal{F}(A, L) e^{-\lambda A} dA = \frac{L}{(2\lambda)^{1/3}} \sum_{k=1}^{\infty} C(\alpha_k)\, e^{-\alpha_k \lambda^{2/3} 2^{-1/3} L}. \tag{63}$$

The constant $C(\alpha_k)$ is given by the expression,

$$C(\alpha_k) = \frac{\left[\int_{-\alpha_k}^{\infty} Ai(z) dz\right]^2}{\int_{-\alpha_k}^{\infty} Ai^2(z) dz} = \frac{\left[\int_{-\alpha_k}^{\infty} Ai(z) dz\right]^2}{Ai'^2(-\alpha_k)}, \tag{64}$$

where we have again used the identity,[28] $\int_{-\alpha_k}^{\infty} Ai^2(z) dz = [Ai'(-\alpha_k)]^2$. Note that $C(\alpha_k) = B^2(\alpha_k)$, where $B(\alpha_k)$ is given in Eq. (21). The constants $C(\alpha_k)$'s can be determined numerically very precisely from Eq. (64) using the Mathematica. As examples, we have determined the first few values in Table I. Note that $C(\alpha_k)$'s oscillate as k increases.

We formally invert the Laplace transform in Eq. (63), take the derivative with respect to h_m and then make a change of variable, $\lambda = sL^{-3/2}$. This leads us to the exact MRH distribution for the free boundary case, $P(h_m, L) = L^{-1/2} F\left(h_m L^{-1/2}\right)$ for all L, where the Laplace transform of the scaling function $F(x)$ is given by

$$\int_0^\infty F(x) e^{-sx} dx = 2^{-1/3} s^{2/3} \sum_{k=1}^{\infty} C(\alpha_k)\, e^{-\alpha_k s^{2/3} 2^{-1/3}} \tag{65}$$

Table I. The second column shows the magnitude α_k of the *k*-th zero of the Airy function *Ai(z)* on the negative real axis upto *k* = 10, obtained using the Mathematica

k	α_k	$C(\alpha_k)$
1	2.33810...	3.30279...
2	4.08794...	1.01282...
3	5.52055...	1.78218...
4	6.78670...	0.90519...
5	7.94413...	1.39473...
6	9.02265...	0.83181...
7	10.04017...	1.19915...
8	11.00852...	0.77846...
9	11.93601...	1.07584...
10	12.82877...	0.73725...

The third column shows the corresponding values of the constant $C(\alpha_k)$ in Eq. (64), again generated via the Mathematica.

with $C(\alpha_k)$'s determined from Eq. (64). One can check from Eq. (65) that the function $F(x)$ is normalized, $\int_0^\infty F(x)dx = 1$.

In order to make contact with the area under a Brownian meander discussed in Section 2.2, we define a new variable $t = 2^{-1/3}s^{2/3}$ and rewrite Eq. (65) as,

$$\int_0^\infty F(x)e^{-\sqrt{2}t^{3/2}x}dx = E\left[e^{-\sqrt{2}t^{3/2}x}\right] = \sum_{k=1}^{\infty} C(\alpha_k)te^{-\alpha_k t}, \tag{66}$$

where E denotes the expectation value with respect to the distribution $F(x)$. Taking a further Laplace transform of Eq. (66) with respect to t we get

$$\int_0^\infty e^{-ut}E\left[e^{-\sqrt{2}t^{3/2}x}\right]dt = \sum_{k=1}^{\infty}\frac{C(\alpha_k)}{(u+\alpha_k)^2} = \frac{\left[\int_u^\infty Ai(z)dz\right]^2}{Ai(u)}. \tag{67}$$

The second equality in Eq. (67) is proved in Appendix-A. Comparing Eq. (67) with Eq. (24) of Section 2.2, one finds that the former is just the square of the latter. Using the result in Eq. (24) and the convolution theorem of Laplace transform, we can then invert the Laplace transform in Eq. (67) to obtain the following result,

$$E\left[e^{-\sqrt{2}t^{3/2}x}\right] = \int_0^t \frac{dt'}{\pi\sqrt{t'(t-t')}}E\left[e^{-\sqrt{2}t'^{3/2}a_1}\right]E\left[e^{-\sqrt{2}(t-t')^{3/2}a_2}\right], \tag{68}$$

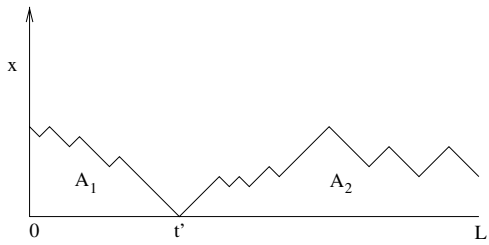

Fig. 5. A stationary profile of the interface $x(\tau)=h_m-h(\tau)$ with the free boundary condition as seen from the maximum h_m located at t'. The point t' divides the path into two statistically independent Brownian meanders with areas A_1 and A_2 respectively.

where a_1 and a_2 are the areas under two independent Brownian meanders each over unit intervals. The result in Eq. (68) is valid for all t. In particular, putting $t=L$ and $x=h_m/\sqrt{L}$, we get

$$E\left[e^{-\sqrt{2}Lh_m}\right]=\int_0^L \frac{dt'}{\pi\sqrt{t'(L-t')}}\, E\left[e^{-\sqrt{2}t'^{3/2}a_1}\right] E\left[e^{-\sqrt{2}(L-t')^{3/2}a_2}\right], \quad (69)$$

which has a very nice and simple physical interpretation. Consider the stationary interface profile over the interval $[0, L]$ after we have made the shift with respect to the maximum, $x(\tau)=h_m-h(\tau)$. A typical picture is shown in Fig. 5.

Let the location of the maximum be denoted by t'. Note that the location $0\leqslant t'\leqslant L$ of the maximum of a free Brownian motion over the interval $[0, L]$ is a random variable whose normalized probability distribution $P(t')$ is well known,[32]

$$P(t')=\frac{1}{\pi\sqrt{t'(L-t')}}, \quad (70)$$

which also describes, in the context of the interface with free boundary conditions, the distribution of the position of the maximum of the interface. It is clear from Fig. 5 that the maximum h_m at t' (or rather the minimum $x=0$ in Fig. 5) divides the path into two Brownian meanders, one over the left interval $[0, t']$ and the other over the right interval $[t', L]$ whose interval length is $(L-t')$. Since a Brownian motion is Markovian, these two meanders are statistically independent of each other. Thus, the areas under the two meanders, $A_1=a_1t'^{3/2}$ and $A_2=a_2(L-t')^{3/2}$ are also statistically independent, except that their joining point t' is distributed

according to Eq. (70). Thus, Eq. (69) has now a probabilistic interpretation,

$$h_m L \equiv \int_0^L \left[A_1(t') + A_2(L-t')\right] P(t') dt', \tag{71}$$

where $P(t')$ is given in Eq. (70). The random variable $h_m L$ has therefore the same law as the sum of the two meander areas (with the location of their joining point t' integrated over with the measure $P(t')$ in Eq. (70)). This result in Eq. (71) for the free boundary condition is thus more involved than its periodic counterpart in Eq. (55).

Moments of the MRH: Using the scaling form, $P(h_m, L) = L^{-1/2} F(h_m L^{-1/2})$ for all L, we get $\langle h_m^n \rangle = \mu_n L^{n/2}$, where $\mu_n = \int_0^\infty F(x) x^n dx$ are the moments of the function $F(x)$ defined in Eq. (65). The computation of μ_n's from Eq. (65) is nontrivial. To make progress, we make use of Eq. (68). We note that the right hand side of Eq. (68) involve the areas a_1 and a_2 of two independent Brownian meanders over unit intervals. Now, the moments associated with the area of a Brownian meander over a unit interval $a_n = E[a^n]$ were computed by a recursive procedure in Section 2.2 and the results are given in Eq. (27). By expanding the exponentials on the right hand side of Eq. (68) in power series and then performing the integral over t' we get

$$E\left[e^{-\sqrt{2}t^{3/2}x}\right] = \frac{1}{\pi} \sum_{n_1=0}^{\infty} \sum_{n_2=0}^{\infty} \frac{(-\sqrt{2})^{n_1+n_2}}{\Gamma(n_1+1)\Gamma(n_2+1)} B\left(\frac{3n_1+1}{2}, \frac{3n_2+1}{2}\right) a_{n_1} a_{n_2} t^{3(n_1+n_2)/2}, \tag{72}$$

where $B(x, y)$ is the standard Beta function and the moments a_n's of the area under a single meander over unit interval were computed in Eq. (27) in Section 2.2. Next, expanding the left hand side of Eq. (72) in a power series and matching identical powers of t, we can express the moment $\mu_n = \int_0^\infty F(x) x^n dx$ in terms of the a_n's,

$$\mu_n = \frac{1}{\pi} \sum_{m=0}^{n} \binom{n}{m} B\left(\frac{3m+1}{2}, \frac{3(n-m)+1}{2}\right) a_m a_{n-m}. \tag{73}$$

Using the known values of a_n's from Eq. (27), one can then recursively determine the moments μ_n from Eq. (73). For example, the first few values are

$$\mu_0 = 1, \quad \mu_1 = \sqrt{\frac{2}{\pi}}, \quad \mu_2 = \frac{17}{24}, \quad \mu_3 = \frac{123}{140}\sqrt{\frac{2}{\pi}}, \ldots \tag{74}$$

Asymptotic tails of the MRH distribution: To determine the asymptotic tails of the MRH distribution, $P(h_m, L) = L^{-1/2} F\left(h_m L^{-1/2}\right)$, we need to know the asymptotic behavior of the scaling function $F(x)$ defined in Eq. (65) in the limits $x \to 0$ and $x \to \infty$. Following similar method as Takacs in the periodic case in Eq. (2), we were able to invert the Laplace transform in Eq. (65) and express it in terms of the hypergeometric function. The derivation is presented in Appendix B. We get,

$$F(x) = \frac{2^{-1/3}}{\sqrt{3\pi}\, x^{7/3}} \sum_{k=1}^{\infty} \alpha_k C(\alpha_k) \left[U\left(1/6, 4/3, b_k/x^2\right) + 2U\left(-5/6, 4/3, b_k/x^2\right) \right] e^{-b_k/x^2}, \tag{75}$$

where $b_k = 2\alpha_k^3/27$, $C(\alpha_k)$ is defined in Eq. (64) and $U(a, b, z)$ is the confluent hypergeometric function. Thus, for the free boundary condition, the scaling function $F(x)$ is different from that of its periodic counterpart namely the Airy distribution function in Eq. (2). The function $F(x)$ appears to be new and hence it lacks a name. We call this function $F(x)$ as the F-Airy distribution function, where F refers to the free boundary condition.

In the limit $x \to 0$, only the $k = 1$ term dominates the sum in Eq. (75) and we get

$$F(x) \to \frac{2\sqrt{2}}{27\sqrt{\pi}} C(\alpha_1) \alpha_1^{7/2} x^{-4} \exp\left[-\frac{2\alpha_1^3}{27x^2} \right], \tag{76}$$

where $\alpha_1 = 2.33810\ldots$ and $C(\alpha_1) = 3.30278\ldots$ from Table I, evaluated using the Mathematica. Thus the function $F(x)$ decays slightly faster as $x \to 0$ than its periodic counterpart in Eq. (56). Finding the asymptotic behavior of $F(x)$ as $x \to \infty$ turns out to be more tricky. However, as in the periodic case, the leading large x behavior can be guessed by analyzing the moment μ_n for large n. It is not difficult to analyze Eq. (73) for large n, knowing the properties of a_n's. We find that for large n, $\mu_n \sim [n/2e]^{n/2}$. Following exactly the same procedure as in the periodic case, we find that $F(x)$ has a leading Gaussian tail for large x,

$$F(x) \sim e^{-3x^2/2}, \tag{77}$$

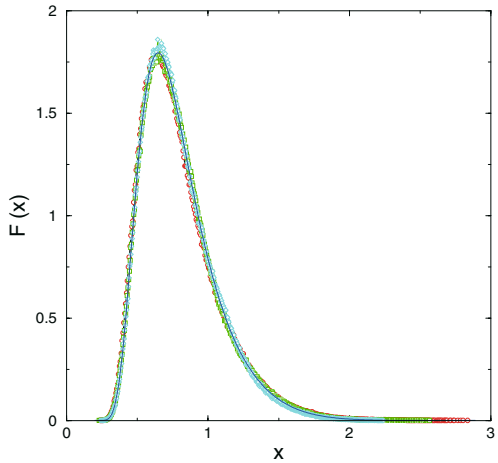

Fig. 6. The scaling function $F(x)$ associated with the MRH distribution, $P(h_m, L) = L^{-1/2}F(h_m/\sqrt{L})$ for the EW equation with free boundary condition. The numerical curves (shown by symbols) are obtained by collapsing the data obtained from the numerical integration of Eq. (58) for three system sizes $L = 256$ (circles), $L = 384$ (squares), and $L = 512$ (diamonds). Also plotted is the Mathematica generated analytical scaling function in Eq. (75) as shown by the solid line.

that falls off less rapidly than the periodic case $f(x) \sim e^{-6x^2}$ in Eq. (57).

Comparison with numerical simulations: Our exact analytical result for the MRH distribution for the free boundary condition is: $P(h_m, L) = L^{-1/2}F\left(h_m L^{-1/2}\right)$ where the scaling function $F(x)$ is given in Eq. (75). We have evaluated the sum in Eq. (75) using the Mathematica. It turns out that the sum is rapidly convergent and it is sufficient to keep terms upto $k = 10$ in the sum. We also numerically integrated the discretized EW Eq. (58) with free boundary condition, i.e., $H(0,t) = H(1,t)$ and $H(L+1,t) = H(L,t)$ and calculated the MRH distribution. In Fig. 6, we compare the analytical scaling function to the one obtained by numerical integration. The number of steps used to reach the stationary state as well as the number of sample averages were the same as in the case of the periodic boundary condition. The numerical data shown in Fig. 6 were obtained by collapsing the histograms for three system sizes $L = 256, 384$, and 512. The agreement is again very good.

5. MRH DISTRIBUTION IN THE STATIONARY REGIME: KPZ INTERFACE

In the previous section, we derived the exact distribution of the MRH in the stationary regime of the $(1+1)$-dimensional EW interface evolving

via Eq. (28). A natural next step would be to extend our method to other $(1+1)$-dimensional interfaces. In this section, we study the MRH distribution in the stationary regime of another very well studied interface that evolves via the nonlinear KPZ equation,[23]

$$\frac{\partial H(x,t)}{\partial t} = \frac{\partial^2 H(x,t)}{\partial x^2} + \lambda \left(\frac{\partial H(x,t)}{\partial x} \right)^2 + \eta(x,t), \tag{78}$$

where $\eta(x,t)$ is a Gaussian white noise with zero mean and a correlator, $\langle \eta(x,t)\eta(x't') \rangle = 2\delta(x-x')\delta(t-t')$. As before, we subtract the zero mode and focus on the relative height, $h(x,t) = H(x,t) - \overline{H(x,t)}$ whose distribution reaches a stationary state in the long time limit in a finite system.

It is well known that the dynamical exponent is $z = 3/2$ for the $(1+1)$-dimensional KPZ equation.[16] Thus, we expect that for times $t >> L^{3/2}$, the system will reach a stationary state. We wish to compute the distribution $P(h_m, L)$ of the MRH, $h_m = \max[\{h\}]$, in this stationary state. In order to compute this distribution, we need to know the stationary joint distribution of the relative heights $P[\{h\}]$ for the KPZ equation. In an infinite system, it is well known[16] that in $(1+1)$-dimensions, the joint distribution of heights approaches a stationary state as $t \to \infty$, where $P[\{H\}] \propto \exp\left[-\frac{1}{2} \int (\partial_x H)^2 dx \right]$. This is a somewhat surprising result since the dependence on the nonlinear term completely drops out of the stationary measure. Indeed, this turns out to be a very special property only valid in $(1+1)$-dimensions. This result can be proved by writing down the full Fokker–Planck equation for the joint height distribution $P[\{H\}, t]$ and then showing explicitly that indeed $P[\{H\}] \propto \exp\left[-\frac{1}{2} \int (\partial_x H)^2 dx \right]$ is a stationary solution of the Fokker–Planck equation.[16] In proving the last step, one neglects various boundary terms that arise out of integration by parts[16] which is justified only in the limit of an infinite system. However, in a finite system, the boundary terms are usually nonzero and it is no longer easy to find the stationary measure.

The only exception seems to be the periodic boundary case where, even in a finite system, the boundary terms can be shown to vanish. Hence in this case the joint distribution of the relative heights $P[\{h\}]$ for the KPZ equation has the same expression as in the EW case, and is given by Eq. (37) with the normalization constant $A_L = \sqrt{2\pi}\, L^{3/2}$. Therefore, for the periodic boundary condition, we expect that the stationary MRH distribution for the KPZ equation will also be identical to that of the EW case, i.e., $P(h_m, L) = L^{-1/2} f\left(h_m L^{-1/2}\right)$ where the scaling function $f(x)$ is the Airy distribution function in Eq. (2).

An interesting challenge is to verify this analytical prediction numerically by directly integrating the KPZ equation (78). The problem is to find an appropriate spatial discretization scheme that will correctly represent the nonlinear term in the continuum Eq. (78). Most of the past studies have used the following natural choice or its simple variants,[33–35]

$$\begin{aligned} H(i,t+\Delta t)-H(i,t) &= \Delta t\,[(H(i+1,t)+H(i-1,t)-2H(i,t)) \\ &\quad +\frac{\lambda}{4}(H(i+1,t)-H(i-1,t))^2\Big]+\eta_i(t)\sqrt{2\Delta t}, \end{aligned} \tag{79}$$

where $\eta_i(t)$'s are independent and identically distributed random variables for each i and t and each drawn from a Gaussian distribution with zero mean and unit variance. However, it is well known[35,36] that certain properties of Eq. (79) are rather unphysical and are fundamentally different from those of the continuum Eq. (78). In other words, the discrete equation (79) fails to capture the correct continuum KPZ evolution.[37] In this paper, we have instead used a discretization scheme proposed by Lam and Shin[38] which circumvents the problems mentioned above. According to this scheme, one uses the Eq. (79) except that the nonlinear term in Eq. (79) is replaced by the following expression,[38]

$$\begin{aligned} &\frac{\lambda}{3}\Big[(H(i+1,t)-H(i,t))^2 \\ &\quad +(H(i+1,t)-H(i,t))(H(i,t)-H(i-1,t))+(H(i,t)-H(i-1,t))^2\Big]. \end{aligned} \tag{80}$$

The advantage with this scheme is that one can prove analytically that the Fokker–Planck equation associated with this discrete model admits a stationary solution for the periodic boundary case,[38] $P[\{H\}]\propto \exp\left[-\frac{1}{2}\sum_{i=1}^{L}(H(i+1)-H(i))^2\right]$ which, in the continuum limit, correctly reproduces the stationary measure of the continuum KPZ equation, i.e., $P[\{H\}]\propto\exp\left[-\frac{1}{2}\int_0^L(\partial_\tau H)^2 d\tau\right]$. We note that a similar but slightly different scheme that also leads to the Gaussian stationary state has been proposed earlier.[39]

We evolved the discretized Eq. (79) (but with the nonlinear term in Eq. (79) replaced by the Lam–Shin nonlinear term in Eq. (80)) with periodic boundary condition and chose $\lambda=1$ and $\Delta t=0.01$. The steady state MRH distribution $P(h_m, L)$ was obtained for three different system sizes

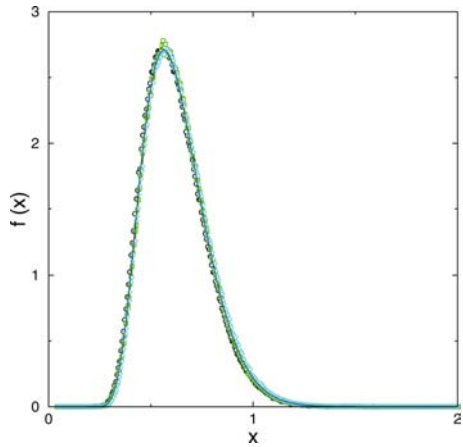

Fig. 7. The scaling function $f(x)$ associated with the MRH distribution, $P(h_m, L) = L^{-1/2} f(h_m/\sqrt{L})$ for the KPZ equation with periodic boundary condition. The numerical curves (shown by symbols) are obtained by collapsing the data obtained from the numerical integration of Eq. (79) (but with the nonlinear term replaced by the Lam–Shin term from Eq. (80)) for three system sizes $L = 256$ (circles), $L = 384$ (squares), and $L = 512$ (diamonds). Also plotted is the Mathematica generated analytical scaling function in Eq. (2) as shown by the solid line.

$L = 256, 384$ and 512. The three data sets were collapsed onto a single scaling plot, $P(h_m, L) = L^{-1/2} f\left(h_m L^{-1/2}\right)$. The numerically obtained scaling function is then compared in Fig. 7 with the analytical scaling function $f(x)$ given in Eq. (2). The agreement is excellent. Thus, for the periodic boundary condition, the stationary MRH distribution of the $(1+1)$-dimensional KPZ equation is also described by the Airy distribution function, as in the case of the EW equation. However, we expect that this superuniversality of the Airy distribution function holds only in $(1+1)$-dimensions, and not in higher dimensions.

We now turn to the case of the free boundary condition, i.e., with Neumann boundary conditions $\partial_x h = 0$ at the two ends $x = 0$ and $x = L$. In the periodic case $P[\{H\}] = \exp\left[-\frac{1}{2}\int (\partial_x H)^2\, dx\right]$ is explicitly the stationary solution of the Fokker–Planck equation. However, for the free boundary case, the same measure is no longer a stationary solution of the Fokker–Planck equation. Thus, unlike in the periodic case where the Airy distribution describing the MRH distribution for the EW equation also describes the MRH distribution of the KPZ equation, for the free boundary case there is no a priori reason to believe that the F-Airy distribution for the EW case will carry over to the KPZ case as well. In fact, as far as we know, the stationary measure for the continuous KPZ equation with the

Neumann boundary condition is still not known explicitly. Thus, calculating analytically the corresponding MRH distribution remains an interesting open problem. Let us also remark about the numerical simulation with free boundary condition. As discussed before in this section, to simulate the continuous KPZ equation one needs to use an appropriate discretization scheme that will reproduce the correct continuum stationary measure. Arbitrary discretization scheme can lead to spurious results. For the periodic boundary condition, such discretization schemes are available thanks to the fact that one knows the stationary state explicitly. For the free boundary case where one does not know the stationary state explicitly, it is a priori not clear what type of discretization schemes one should use.

In fact, to study the effects of different boundary conditions on the MRH distribution in nonlinear KPZ type interfaces, it may be more appropriate and easier to study the discrete growth models that belong to the KPZ universality class, rather than the continuous KPZ equation itself. Several such models are known,[40] an example being the single-step model.[41] This single-step model can further be mapped to the asymmetric exclusion process (ASEP). A particle at a site i in ASEP corresponds to a downward slope of the interface height on one unit and a hole in ASEP corresponds to an upward slope of the interface step of one unit. The height $h_i(t)$ at site i in the interface model is thus related to the occupancy τ_i in ASEP via the simple relation, $h_{i+1}(t) - h_i(t) = 1 - 2\tau_i(t)$ where $\tau_i = 1$ (or 0) if the site i is occupied (or empty) in the ASEP. Over the past few years there have been extensive studies of ASEP with open boundary conditions where a particle enters the lattice through its left end at rate α and leaves the lattice through its right boundary at rate β.[42] Several steady state properties of this system are known.[43] The open boundary conditions in ASEP means special growth rules at the boundaries of the interface model. Thus, many results from the ASEP can then be used to predict the properties of the interface model with special boundary conditions.[43] In particular, for $\alpha \leqslant 1$, $\beta \leqslant 1$ and on the line $\alpha + \beta = 1$, ASEP is known to have a factorized steady state, i.e., the τ_i's become independent from site to site, each with a bivariate distribution $p(\tau) = \alpha\delta_{\tau,1} + \beta\delta_{\tau,0}$. This means that the slope variables in the corresponding interface model also get uncorrelated in the stationary state. The stationary profile in space is then described by a one dimension random walk with drift, $h_{i+1} - h_i = \xi_i$ where ξ_i's are i.i.d variables which take the value 1 (with probability $\beta = 1 - \alpha$) and -1 (with probability α). Thus, we have a random walk with a drift $\mu = 1 - 2\alpha$. For the zero drift case, $\alpha = \beta = 1/2$, we would then expect that the F-Airy distribution function, upto a scale factor, would describe the MRH distribution of the interface in the continuum limit. It would be

interesting to extend the method presented here to calculate the MRH distribution for $\mu \neq 0$.

6. MRH DISTRIBUTION OF INTERFACES IN THE GROWING REGIME

In this section, we discuss the MRH distribution of a $(1+1)$-dimensional interface in its growing regime, i.e., when the time $1 << t << L^z$ where z is the dynamical exponent associated with the growth. The MRH distribution in the growing regime turns out to be more universal than its stationary counterpart and holds for generic interfaces. Logically, one would have preferred to discuss the growing regime (early time) before the stationary regime (late time). However, we will need to use some of the results for the stationary regime derived in Section 4 in our discussion of the MRH distribution in the growing regime. Hence is the reversal of the order. The MRH distribution in the growing regime has been discussed previously in ref. 21 and we will be using a similar line of arguments. Nevertheless, we decided to include this section partly because our results would be more precise and partly to make this paper self-contained and complete.

Let us consider a growing interface starting from a flat initial condition at $t = 0$. Initially the heights are completely uncorrelated. As time grows, the correlation between heights also grow. As discussed in Section 3, at any finite time t, the height–height correlation function decays with spatial distance over a characteristic correlation length $\xi(t)$ which grows algebraically with time, $\xi(t) \sim t^{1/z}$. In the growing regime when the time $1 << t << L^z$, this correlation length is much smaller than the system size, $\xi(t) << L$. Thus, one can break up the whole system of size L into $N = L/\xi$ blocks each of size $\xi(t)$, as shown in Fig. 8. The heights (or rather the relative heights) at two points belonging to two different blocks are basically uncorrelated since the distance between them is bigger than the correlation length $\xi(t)$. However, inside a given block, the heights are strongly correlated. Let us denote the MRH in block i by $h_m(i)$. These block MRH's are shown by the black dots in Fig. 8.

We are interested in the distribution of the *global* MRH, $h_m = \max[h_m(1), h_m(2), \ldots, h_m(N)]$ where N is the number of blocks. Since the block variables $h_m(i)$'s are uncorrelated, we are thus interested in the extreme value statistics of a set of N uncorrelated random variables, a subject that has been rather well studied.[17] Furthermore, since $\xi(t) << L$, the system does not feel the presence of the boundaries and there is a translational invariance over the block index i. This indicates that the random variables $h_m(i)$'s associated with different blocks are not just independent, but share the same distribution as well. Let us denote this

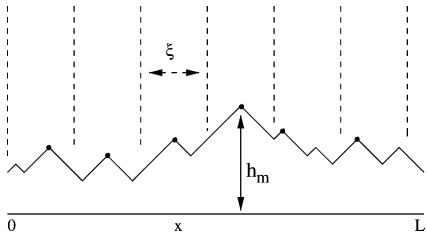

Fig. 8. An interface in the growing regime with correlation length $\xi(t)$. The system is divided into $N = L/\xi(t)$ blocks each of length $\xi(t)$. The heights in different blocks are essentially uncorrelated. The MRH in each block is denoted by a black dot. Also shown is the global maximal relative height h_m.

common distribution by $\rho(x,\xi) = \text{Prob}[h_m(i) = x, \xi]$, where ξ is the size of the block. Due to the independence of different blocks, the joint distribution $P[\{h_m(i)\}]$ of the block variables $h_m(i)$'s factorize, $P[\{h_m(i)\}] = \prod_i \rho(h_m(i), \xi)$.

To guess the form of the distribution $\rho(x,\xi) = \text{Prob}[h_m(i) = x, \xi]$, one makes a reasonable assumption that within a given block of size ξ, the heights have already reached the stationary state even though the full system is still in the growing regime. Then $\rho(x)$ is just given by the stationary MRH distribution with a system size ξ and one can then directly use the results obtained in the previous section, namely the scaling form, $\rho(x,\xi) = \xi^{-1/2} W\left(x\,\xi^{-1/2}\right)$. More generally, one should use the scaling form, $\rho(x,\xi) = \xi^{-\alpha} W\left(x\,\xi^{-\alpha}\right)$, where α is the roughness exponent of the surface. For the $(1+1)$-dimensional EW and the KPZ equation, one has $\alpha = 1/2$. The roughness exponent α is related to the dynamical exponent z and the growth exponent β via the simple scaling law, $\alpha = \beta z$.[16] Note that the scaling function $W(x)$ depends on the boundary condition. For the periodic boundary case, we had $W(x) = f(x)$ where $f(x)$ is the Airy distribution function in Eq. (2). For the free boundary condition, at least for the EW interface, $W(x) = F(x)$ with $F(x)$ being the F-Airy distribution function in Eq. (75). Note that it is not easy to guess the boundary conditions at the edges of a block of size ξ. Therefore, it is difficult to know the precise form of the scaling function $W(x)$. However, it turns out that in the scaling regime (see later), only the large x behavior of $W(x)$ matters. Now, both for the periodic (EW and KPZ) and the free boundary conditions (only EW), we have seen in Eqs. (57) and (77) that the scaling function $W(x)$ has a Gaussian tail for large x,

$$W(x) \sim \exp\left[-bx^2\right], \tag{81}$$

where the constant $b=6$ for the periodic case and $b=3/2$ for the free case. This suggests that the large x tail of the scaling function is generically Gaussian, though the constant b is nonuniversal and depends on the details of the boundary conditions.

Let us first define the cumulative distribution of the global MRH in a system of size L and at time t,

$$F(h_m, L, t) = \text{Prob}\,[\max\{h_m(1), h_m(2), \ldots, h_m(N)\} < h_m,\ L,\ t]. \quad (82)$$

Using the fact that the block MRH $h_m(i)$'s have a factorised joint distribution, it then follows that

$$F(h_m, L, t) = \left[\int_{-\infty}^{h_m} \rho(z, \xi)\, dz\right]^N = \left[1 - \int_{h_m}^{\infty} \rho(z, \xi)\, dz\right]^N. \quad (83)$$

Substituting the scaling form, $\rho(x, \xi) = \xi^{-\alpha}\, W(x\,\xi^{-\alpha})$ in Eq. (83) we get

$$F(h_m, L, t) = \left[1 - \int_{h_m/\xi^{\alpha}}^{\infty} W(y)\, dy\right]^N \approx \exp\left[-N \int_{h_m/\xi^{\alpha}}^{\infty} W(y)\, dy\right], \quad (84)$$

where the last equality holds near the tail $h_m \to \infty$. Using the Gaussian behavior of $W(x)$ for large x in Eq. (81), it is easy to analyze the integral inside the exponential in Eq. (84) and one arrives at the limiting distribution,

$$F(h_m, L, t) \to V\left(c\,\frac{D_L}{\xi^{2\alpha}}\,(h_m - D_L)\right), \text{ with } V(y) = \exp\left[-e^{-y}\right], \quad (85)$$

where $D_L = \xi^{\alpha}\sqrt{\log(L/\xi)}$, c is an unimportant nonuniversal constant and the scaling function $V(y)$ is the celebrated Gumbel function. The probability distribution of the global MRH is then obtained by taking the derivative in Eq. (85), $P(h_m, L, t) = \partial F(h_m, L, t)/\partial h_m$. This distribution is clearly peaked around its average value,

$$\langle h_m(t)\rangle \sim \xi^{\alpha}\sqrt{\log(L/\xi)} \sim t^{\beta}\left[\log(L\,t^{-1/z})\right]^{1/2}. \quad (86)$$

The width of the peak around this average can also be read off Eq. (85)

$$w = \sqrt{\langle h_m^2\rangle - \langle h_m\rangle^2} \sim \frac{\xi^{2\alpha}}{D_L} \sim t^{\beta}\left[\log(L\,t^{-1/z})\right]^{-1/2}. \quad (87)$$

For the $(1+1)$-dimensional EW equation, $z=2$, $\beta=1/4$ and for the KPZ equation, $z=3/2$, $\beta=1/3$. The result for the average in Eq. (86) was also obtained in ref. 21, though the power $1/2$ of the logarithm in Eq. (86) was found only numerically. In our case, this power $1/2$ is a direct consequence of the large x Gaussian tail of the scaling function $W(x)$ in Eq. (81), which were derived analytically for the EW and the KPZ equation in Section 4 and 5. Thus, the main conclusion of this section is that in the growing regime, the appropriately scaled global MRH has the universal Gumbel distribution that does not depend on the details of the interface.

7. CONCLUSION

To summarize, in this paper we have studied the distribution of the global maximum h_m of relative heights (i.e., the height measured with respect to the spatially averaged height) in $(1+1)$-dimensional fluctuating interfaces, both of the EW and the KPZ variety. The distribution $P(h_m, L, t)$, at time t and in a system of size L, has two types of scaling behaviors depending on whether one is in the *growing regime* (where $1 << t << L^z$) or in the *stationary regime* (where $t >> L^z$), z being the dynamical exponent of the interface. In the growing regime, the distribution (appropriately scaled) is described by the universal Gumbel law of the extreme value statistics. On the other hand, in the stationary regime, the distribution becomes time independent and has the scaling form, $P(h_m, L) = L^{-1/2} W\left(h_m L^{-1/2}\right)$. The scaling function $W(x)$ depends on the boundary condition. For the periodic boundary condition, we have analytically shown that $W(x) = f(x)$ where $f(x)$ is the Airy distribution function in Eq. (2) that describes the distribution of the area under a Brownian excursion over a unit interval. In fact, in this case, the EW and the KPZ interface both share the same scaling function $f(x)$. In the case of the free boundary condition, we have shown that for the EW interface, $W(x) = F(x)$ where $F(x)$ is the F-Airy distribution function defined in Eq. (75). These analytical results have also been verified by numerical integration of the EW and the KPZ equations. These results are summarized in Fig. 9. Since the relative heights in the stationary state are strongly correlated, our results provide a rather rare exactly solvable case for the distribution of extremum of a set of *correlated* random variables.

Our work shows that there is yet another nontrivial scaling function in the $(1+1)$-dimensional KPZ equation, namely the Airy distribution function that appears in the stationary MRH distribution in $(1+1)$-dimensional KPZ equation with periodic boundary condition. Note that several

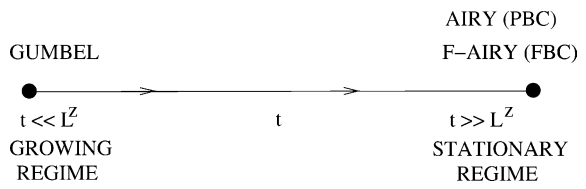

Fig. 9. As time t increases, the scaled MRH distribution crosses over from the universal Gumbel form in the growing regime to either the Airy distribution function (for the periodic boundary condition (PBC)) or to the F-Airy distribution function (for the free boundary condition (FBC)) in the stationary regime.

other nontrivial scaling functions have appeared before in $(1+1)$-dimensional KPZ equation. Let us list a few.

(i) In the steady state of the one dimensional EW or the KPZ equation, the width of the surface height defined as

$$w^2 = \frac{1}{L}\int_0^L H^2(x,t)dx - \frac{1}{L^2}\left[\int_0^L H(x,t)dx\right]^2, \tag{88}$$

was shown to have a scaling distribution, $P(w^2) \simeq \langle w^2\rangle^{-1}\,\Phi(w^2/\langle w^2\rangle)$ where the scaling function $\Phi(x)$ is nontrivial.[29]

(ii) For the $(1+1)$-dimensional KPZ equation, the probability distribution of the spatially integrated height $Y_t = \int_0^L H(x,t)dx$, i.e., the area under the surface profile, was shown to have the following behavior at late times t[44]

$$P(Y_t) \sim \exp[t\,Z_L\,(Y_t/t)], \tag{89}$$

where $Z_L(x)$ is a large deviation function which has a Gaussian peak near $x=0$, but has highly non-Gaussian and asymmetric tails for large $|x|$.

(iii) More recently, it has been shown[45] that the single site height distribution $P(H,t)$ in the growing regime $t << L^{3/2}$ of the $(1+1)$-dimensional KPZ equation scales as

$$P(H,t) \sim t^{-1/3} T_W\left(\frac{H-\langle H\rangle}{t^{1/3}}\right), \tag{90}$$

where the scaling function $T_W(x)$ is identical (upto a scale factor) to the celebrated Tracy–Widom distribution for the largest eigenvalue of a random matrix drawn from the Gaussian unitary ensemble.[46] Note that in

the stationary regime $t >> L^{3/2}$, this single site height distribution becomes a simple Gaussian. However, as demonstrated in this paper, the global maximum of all these heights in a finite system of size L has a nontrivial distribution in the stationary regime, characterized by the Airy distribution function for the periodic boundary condition case. Determining the corresponding scaling function in the KPZ equation in a finite system with free boundary conditions remains an open problem.

In this paper we have analytically studied the distribution of the extreme height fluctuations in the stationary state of a $(1+1)$-dimensional interface. These height fluctuations are strongly correlated in the stationary state. Thus our work provides a rare example where one can calculate exactly the extreme value distribution of a set of strongly correlated random variables. In the context of interfaces, it is worth pointing out that another type of extreme statistics has been studied recently.[47] In ref. 47 the authors study the distribution of the maximum of the Fourier modes of the height fluctuations. However, in this case the Fourier modes are independent of each other and the analytical computation is simpler, though physically relevant.

Experimental Consequences: Our work opens up an interesting experimental challenge to measure the Airy (or the F-Airy) distribution function in a physical system. Many experimental systems are known to be well described by the $(1 + 1)$-dimensional EW eq. (28). Examples include, amongst others, the high-temperature step fluctuations in crystal surfaces[48,49] and the displacements of nonmagnetic particles in dipolar chains at low magnetic field.[50] In fact, in the former system, there have been beautiful recent measurements of a variety of interface properties such as various first-passage properties,[48] which were studied before only theoretically.[51] Hence, it would be interesting to see if the MRH distribution can also be measured in these experimental systems. This would then be the first experimental measurement of the Airy distribution function which has so far appeared only in mathematical problems.

Several new directions and interesting open questions emerge from this work. One of the challenges is to calculate the MRH distribution for interfaces in higher dimensions. For example, let us consider the $(d+1)$-dimensional EW equation, where the Laplacian term in the EW equation is d-dimensional. This equation for $d > 2$ describes several interesting systems, e.g., a fluctuating random Gaussian manifold and also the time evolution of the magnetization of a spin system within mean field theory (for $d > 4$). It is simpler to continue to think in terms of interface heights growing over a d-dimensional substrate. The relative heights will again reach a stationary joint distribution function in the long time limit,

$$P[\{h(\vec{r})\}] \propto e^{-\frac{1}{2}\int (\nabla h)^2 d\vec{r}}\, \delta\left[\int h(\vec{r}) d\vec{r}\right]. \tag{91}$$

The calculation of the distribution of the MRH h_m, starting from the above joint distribution, is a theoretical challenge. For $d < 2$, the surface will be rough in the stationary state and one expects that the MRH will scale as, $h_m \sim L^{\alpha}$ where $\alpha = 1 - d/2$ is the roughness exponent and L is the linear size of the substrate. Hence, the MRH distribution is expected to have the scaling form, $P(h_m, L) \sim L^{-\alpha} f_d\left(h_m L^{-\alpha}\right)$ where the scaling function $f_d(x)$ will depend explicitly on the dimension d. On the other hand, for $d > 2$, the surface is smooth and $h_m \sim O(1)$ even in the thermodynamic limit $L \to \infty$. Hence, $P(h_m, L)$ will approach a limiting distribution $P(h_m)$ in the thermodynamic limit. It would be interesting to compute this limiting distribution for $d > 2$. This is nontrivial because the relative heights are still correlated (the correlation function falls off only as a power law $1/r^{d-2}$), even though the surface is smooth. The only simplification happens in the limit of $d \to \infty$, where the correlation function dampens exponentially and one would expect, using the theory of extreme value statistics of independent random variables as in Section 6, a Gumbel distribution for $P(h_m)$. In fact, this has recently been verified for the EW interface defined on a small world network.[52] However, for finite $d > 1$, the problem is wide open. The path integral techniques used in this paper are suitable only in one dimension. Entirely new techniques are required to deal with the problem in higher dimensions. Developments of such techniques are more than welcome.

APPENDIX A: DERIVATION OF TWO IDENTITIES

In this appendix, we prove two identities,

$$\sum_{k=1}^{\infty} \frac{B(\alpha_k)}{(\alpha_k + u)} = \frac{\int_u^{\infty} Ai(z) dz}{Ai(u)}, \tag{A.1}$$

$$\sum_{k=1}^{\infty} \frac{B^2(\alpha_k)}{(\alpha_k + u)^2} = \left[\frac{\int_u^{\infty} Ai(z) dz}{Ai(u)}\right]^2, \tag{A.2}$$

where α_k's are the magnitude of the zeros of the Airy function $Ai(z)$ on the negative real axis, i.e., $Ai(-\alpha_k) = 0$ and $B(\alpha_k)$ is given by

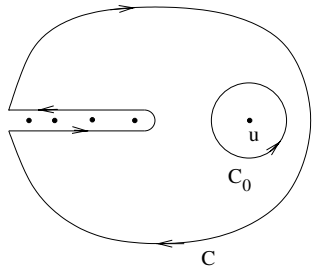

Fig. 10. The contour for the integral in Eq. (A.4). The dots on the negative real axis denote the zeros $-\alpha_k$'s of the Airy function $Ai(z)$.

$$B(\alpha_k) = \frac{\int_{-\alpha_k}^{\infty} Ai(z)dz}{Ai'(-\alpha_k)}, \tag{A.3}$$

where $Ai'(z) = dAi(z)/dz$. The first identity was used in Eq. (24). The second identity appeared in Eq. (67) where $C(\alpha_k) = B^2(\alpha_k)$.

To prove the first identity in Eq. (A.1), we consider the following contour integral in the complex z plane,

$$I_1 = \int_C \frac{dz}{2\pi i} \frac{1}{(z-u)} \frac{\int_z^{\infty} Ai(z')dz'}{Ai(z)}, \tag{A.4}$$

where the contour C is shown in Fig. 10. Note that the integrand in Eq. (A.4) has simple poles at $z = u$ and $z = -\alpha_k$ for $k = 1, 2, \ldots$. The latter fact follows since $-\alpha_k$ is a simple zero of $Ai(z)$.

Using the asymptotic expansion of $Ai(z) \sim z^{-1/4} \exp[-2z^{2/3}/3]$ for large z,[4] it is easy to see that the function $Q(z) = \int_z^{\infty} Ai(z')dz'/Ai(z) \sim z^{-1/2}$ for large z. Hence, once we extend the radius of the contour C to infinity, the contribution to the integral I_1 in Eq. (A.4) from the circular part of the contour tends to zero. The only remaining contribution comes from the arms of the contour around the negative real axis, which is equal to the sum of the residues around $-\alpha_k$'s each of which is a simple pole of the function $Q(z)$. Evaluating the residues around these poles in Eq. (A.4) we get

$$I_1 = -\sum_{k=1}^{\infty} \frac{B(\alpha_k)}{(\alpha_k + u)}. \tag{A.5}$$

On the other hand, since the integrand in Eq. (A.4) is analytic in the interior of the domain between the contour C and C_0 in Fig. 10, it follows

that $\int_C = -\int_{C_0}$. But the integral around C_0 is just the residue at the pole $z=u$. Evaluating this residue, we then get

$$I_1 = -\frac{\int_u^\infty Ai(z)dz}{Ai(u)}. \tag{A.6}$$

Comparing Eqs. (A.5) and (A.6), we get the identity in Eq. (A.1).

The identity in Eq. (A.2) can be proved exactly in the same manner. We now consider the contour integral,

$$I_2 = \int_C \frac{dz}{2\pi i}\,\frac{1}{(z-u)}\left[\frac{\int_z^\infty Ai(z')dz'}{Ai(z)}\right]^2, \tag{A.7}$$

around the same contour C in Fig. 10. Note that the integrand in Eq. (A.7) now has doubles poles at $z=-\alpha_k$ for all $k=1,2,\ldots$ (apart from the single pole at $z=u$). The rest of the calculation is similar as in the evaluation of I_1 and we do not repeat them here. Following these steps one easily arrives at the identity in Eq. (A.2).

APPENDIX B: THE INVERSION OF A LAPLACE TRANSFORM

In this appendix, we wish to express the function $F(x)$ explicitly in real space x by inverting its Laplace transform,

$$\int_0^\infty F(x)\,e^{-sx}dx = 2^{-1/3}s^{2/3}\sum_{k=1}^{\infty} C(\alpha_k)\,e^{-\alpha_k s^{2/3}2^{-1/3}}, \tag{B.1}$$

where the constant, $C(\alpha_k)=[B(\alpha_k)]^2$ with $B(\alpha_k)$ given in Eq. (A.3).

To proceed, we use an identity originally derived by Takacs in the context of Brownian excursions,[3]

$$2^{1/3}\int_0^\infty J\left(2^{1/3}x^{-2/3}\right)x^{-5/3}e^{-sx}dx = e^{-s^{2/3}}, \tag{B.2}$$

where the function $J(x)$ can be expressed in terms of the known hypergeometric function $U(a,b,z)$,

$$J(x) = \frac{2^{2/3}x}{3^{3/2}\sqrt{\pi}}\,U\left(1/6, 4/3, 2x^3/27\right)e^{-2x^3/27}. \tag{B.3}$$

Thus the identity in Eq. (B.2) gives us the inverse Laplace transform,

$$\mathcal{L}_s^{-1}\left[e^{-s^{2/3}}\right]=2^{1/3}x^{-5/3}J\left(2^{1/3}x^{-2/3}\right), \tag{B.4}$$

where $J(x)$ is given by Eq. (B.3).

Our first step is to rescale s in Eq. (B.4) by a constant factor, i.e., $s\to\gamma^{3/2}s$. This is equivalent to the rescaling, $x\to\gamma^{-3/2}x$. Then, Eq. (B.4) transforms into

$$\mathcal{L}_s^{-1}\left[e^{-\gamma s^{2/3}}\right]=\gamma\,2^{1/3}x^{-5/3}J\left(\gamma 2^{1/3}x^{-2/3}\right). \tag{B.5}$$

Differentiating Eq. (B.5) with respect to γ gives

$$\mathcal{L}_s^{-1}\left[2^{-1/3}s^{2/3}e^{-\gamma s^{2/3}}\right]=-x^{-5/3}J\left(2^{1/3}x^{-2/3}\right)-\gamma 2^{1/3}x^{-7/3}J'\left(\gamma 2^{1/3}x^{-2/3}\right), \tag{B.6}$$

where $J'(x)=dJ/dx$. We take the derivative of the function $J(x)$ in Eq. (B.3) and use the following identity[4] satisfied by the function $U(a,b,x)$

$$x\frac{\partial U(a,b,x)}{\partial x}=(a-b+x)\,U(a,b,x)-U(a-1,b,x). \tag{B.7}$$

Rearranging and simplifying, we get

$$\mathcal{L}_s^{-1}\left[2^{-1/3}s^{2/3}e^{-\gamma s^{2/3}}\right]=\frac{\gamma}{\sqrt{3\pi}\,x^{7/3}}\left[U\left(1/2,4/3,4\gamma^3/27x^2\right)+2U\left(-5/6,4/3,4\gamma^3/27x^2\right)\right]e^{-4\gamma^3/27x^2}. \tag{B.8}$$

Note that this formula in Eq. (B.8) is exactly what we need to invert the Laplace transform in Eq. (B.1). Substituting $\gamma=2^{-1/3}\alpha_k$ in Eq. (B.8) and using this formula in Eq. (B.1) we get

$$F(x)=\frac{2^{-1/3}}{\sqrt{3\pi}x^{7/3}}\sum_{k=1}^{\infty}\alpha_k C(\alpha_k)\left[U\left(1/6,4/3,b_k/x^2\right)+2U\left(-5/6,4/3,b_k/x^2\right)\right]e^{-b_k/x^2}, \tag{B.9}$$

where $b_k=2\alpha_k^3/27$.

REFERENCES

1. D. A. Darling, On the supremum of certain Gaussian processes, *Ann. Prob.* **11**:803–806 (1983).
2. G. Louchard, Kac's formula, Levy's local time and Brownian excursion, *J. Appl. Prob.* **21**:479–499 (1984).
3. L. Takacs, A Bernoulli excursion and its various applications, *Adv. Appl. Prob.* **23**:557–585, (1991); Limit distributions for the Bernoulli meander, *J. Appl. Prob.* **32**:375–395 (1995).
4. M. Abramowitz and I. A. Stegun, *Handbook of Mathematical Functions* (Dover, New York, 1973).
5. M. Csörgö, Z. Shi, and M. Yor, Some asymptotic properties of the local time of the uniform empirical processes, *Bernoulli* **5**:1035–1058 (1999).
6. P. Flajolet, P. Poblete, and A. Viola, On the analysis of linear probing hashing, *Algorithmica* **22**:490–515 (1998).
7. P. Flajolet and G. Louchard, Analytic variations on the Airy distribution, *Algorithmica* **31**:361–377 (2001).
8. P. Flajolet, B. Salvy, and G. Schaeffer, Airy phenomena and analytic combinatorics of connected graphs, *Electron. J. Combin.* **11**:1–30 (2004).
9. C. L. Mallows and J. Riordan, The inversion enumerator for labelled trees, *Bull. Am. Math. Soc.* **74**:92–94 (1968); I. Gessel, B. E. Sagan, and Y.-N. Yeh, Enumeration of trees by inversion, *J. Graph Theory* **19**:435–459 (1995).
10. E. M. Wright, The number of connected sparsely edged graphs, *J. Graph Theory* **1**:317–330 (1977); 2- Smooth graphs and blocks **2**:299–305 (1978); 3-Asymptotic results **4**:393–407 (1980).
11. P. Flajolet, D. E. Knuth, and B. Pittel, The first cycles in an evolving graph, *Discrete Math.* **75**:167–215 (1989); S. Janson, D. E. Knuth, T. Luczak, and B. Pittel, *Random Struct and Algorithms* **4**:233 (1993).
12. C. Richard, A. J. Guttmann, and I. Jensen, Scaling function and universal amplitude combinations for self avoiding polygons, *J. Phys. A: Math. Gen.* **34**:L495–501 (2001); C. Richard, Scaling behaviour of the two-dimensional polygons models, *J. Stat. Phys.* **108**:459–493 (2002); C. Richard, I. Jensen, and A. J. Guttmann, Scaling function for self-avoiding polygons, *Proceedings of the International Congress on Theoretical Physics, Paris, July 2002, D. Iagolnitzer, D. Rivasseau, and J. Zinn-Justin*, eds. (Birkhauser), cond-mat/0302513.
13. C. Richard, Area distribution of the planar random loop boundary, *J. Phys. A: Math. Gen.* **37**:4493–4500 (2004).
14. S. N. Majumdar and A. Comtet, Exact maximal height distribution of fluctuating interfaces, *Phys. Rev. Lett.* **92**:225501 (2004).
15. A. L. Barabasi and H. E. Stanley, *Fractal Concepts in Surface Growth* (Cambridge University Press, Cambridge, England, 1995); J. Krug, *Adv. Phys.* **46**:139–282 (1997).
16. T. Halpin-Healy and Y.-C. Zhang, Kinetic roughening phenomena, stochastic growth, directed polymers and all that, *Phys. Rep.* **254**:215–414 (1995).
17. E. J. Gumbel, *Statistics of Extremes* (Columbia University Press, New York, 1958).
18. J.-P. Bouchaud and M. Mézard, Universality classes for extreme value statistics, *J. Phys. A* **30**:7997–8015 (1997); D. Carpentier and P. Le Doussal, Glass transition of a particle in a random potential, front selection in non-linear renormalization group and entropic phenomena in Liouville and sinh-Gordon models, *Phys. Rev. E* **63**:026110 (2001); D. S. Dean and S. N. Majumdar, Extreme-value statistics of hierarchically correlated variables, deviation from Gumbel statistics and anomalous persistence, *Phys. Rev. E*

64:046121 (2001); P. LeDoussal and C. Monthus, Exact solutions for the statistics of extrema of some random 1D landscapes, application to the equilibrium and the dynamics of the toy model, *Physica A* **317**:140–198 (2003).
19. For a review see, S. N. Majumdar and P. L. Krapivsky, Extreme value statistics and traveling fronts: various applications, *Physica A* **318**:161–170 (2003).
20. For a review see, E. Ben-Naim, P. L. Krapivsky, and S. Redner, extremal properties of random structures, cond-mat/0311552.
21. S. Raychaudhuri, M. Cranston, C. Przybyla, and Y. Shapir, Maximal height scaling of kinetically growing surfaces, *Phys. Rev. Lett.* **87**:136101 (2001).
22. S. F. Edwards and D. R. Wilkinson, The surface statistics of a granular agregate, *Proc. R. Soc. London A* **381**:17–31 (1982).
23. M. Kardar, G. Parisi and Y.-C. Zhang, Dynamical scaling of growing interfaces, *Phys. Rev. Lett.* **56**:889–892 (1986).
24. M. Perman and J.A. Wellner, On the distribution of Brownian areas, *Ann. Appl. Prob.* **6**:1091–1111 (1996).
25. M. Jeanblanc, J. Pitman and M. Yor, The Feynman–Kac formula and decomposition of Brownian paths, *Comput. Appl. Math.* **16**:27–52 (1997).
26. M. Nguyen Thê, Area and inertial moments of Dyck paths, Combinatorics, Probability and Computing (2003), submitted.
27. S. Redner, *A Guide to First-passage Processes* (Cambridge University Press, Cambridge 2001).
28. J.R. Albright, Integrals of products of Airy functions, *J. Phys. A* **10**:485–490 (1977).
29. G. Foltin, K. Oerding, Z. Racz, R. L. Workman, and R. K. P. Zia, Width distribution for random-walk interfaces, *Phys. Rev. E* **50**:R639–642 (1994); Z. Racz and M. Plischke, Width distribution for 2+1 dimensional growth and deposition processes, *Phys. Rev. E* **50**:3530–3537 (1994).
30. T. W. Burkhardt, Semiflexible polymer in the half plane and statistics of the integral of a Brownian curve, *J. Phys. A* **26**:L1157–1162 (1993).
31. A. Yu. Grosberg and A. R. Khokhlov, *Statistical Physics of Macromolecules* (AIP Press, 1994).
32. W. Feller, *Introduction to Probability Theory and its Applications*, 3rd ed., Vol. I. (Wiley, New York, 1968).
33. J. Amar and F. Family, Numerical solution of continuum equation for interface growth in 2+1 dimension, *Phys. Rev. A* **41**:3399–3402 (1990).
34. K. Moser, J. Kertész, and D. E. Wolf, Numerical solution of the Kardar–Parisi–Zhang equation in one,two and three dimensions, *Physica A* **178**:215–226 (1991); K. Moser and D. E. Wolf, Vectorized and parallel simulations of the Kardar–Parisi–Zhang equation in 3+1 dimensions, *J. Phys. A* **27**:4049–4054 (1994).
35. C. Dasgupta, S. Das Sarma, and J. M. Kim, Controlled instability and multiscaling in models of epitaxial growth, *Phys. Rev. E* **54**:R4552–4555 (1996); C. Dasgupta, J. M. Kim, M. Dutta, and S. Das Sarma, Instability, intermittency, and multiscaling in discrete growth models of kinetic roughening, ibid. **55**:2235–2254 (1997).
36. T. J. Newman and A. J. Bray, Strong coupling behaviour in discrete Kardar–Parisi–Zhang equation, *J. Phys. A* **29**:7917–7928 (1996).
37. C.-H. Lam and F. G. Shin, Anomaly in numerical integration of the Kardar–Parisi–Zhang equation, *Phys. Rev. E* **57**:6506–6511 (1998).
38. C.-H. Lam and F. G. Shin, Improved discretisation of the Kardar–Parisi–Zhang equation, *Phys. Rev. E* **58**:5592–5595 (1998).
39. See Eq. (5.26) in ref. 40 where this result was attributed to unpublished work (1989) of T. Nieuwenhuizen.

40. For a review, see J. Krug and H. Spohn, in *Solids Far From Equilibrium: Growth, Morphology and Defects*, C. Godreche, ed. (Cambridge University Press, Cambridge, 1991).
41. P. Meakin *et al.*, Ballistic deposition on surfaces, *Phys. Rev. A* **34**:5091 (1986).
42. B. Derrida *et. al.*, Exact solution of a 1-d asymmetric exclusion model using a matrix formulation, *J. Phys. A* **26**:1493 (1993).
43. For a review, see B. Derrida and M. R. Evans in *Nonequilibrium Statistical Mechanics in One Dimension*, V. Privman, ed. (Cambridge University Press, Cambridge, 1997).
44. B. Derrida and J. L. Lebowitz, Exact large deviation function in the asymmetric exclusion process, *Phys. Rev. Lett.* **80**:209–213 (1998); B. Derrida and C. Appert, Universal large deviation function of the Kardar–Parisi–Zhang equation in one dimension, *J. Stat. Phys.* **94**:1–30 (1999).
45. M. Praehofer and H. Spohn, Universal distribution of growth processes in 1+1 dimensions and random matrices, *Phys. Rev. Lett.* **84**:4882–4885 (2000); Exact scaling function for one-dimensional stationary KPZ growth, *J. Stat. Phys.* **115**:255–279 (2002). K. Johansson, Shape fluctuations and random matrices *Commun. Math. Phys.* **209**:437–476 (2000); J. Gravner, C. A. Tracy and H. Widom, Limit theorems for height fluctuations in a class of discrete space and time growth models *J. Stat. Phys.* **102**:1085–1132 (2001); S. N. Majumdar and S. Nechaev, Anisotropic ballistic deposition model with links to the Ulam problem and the Tracy–Widom distribution, *Phys. Rev. E* **69**:011103 (2003); P. L. Ferrari, Ploynuclear growth on a flat substrate and edge scaling of GOE eigenvalues, *Comm. Math. Phys.* **252**:77–109 (2004); T. Imamura and T. Sasamoto, Fluctuations of a one-dimensional polynuclear growth model in a half space, *J. Stat. Phys.* **115**:749–803 (2004).
46. C. A. Tracy and H. Widom, Level-spacing distributions and the Airy kernel, *Commun. Math. Phys.* **159**:151–174 (1994).
47. G. Gyorgyi *et al.*, Statistics of extreme intensities for Gaussian interfaces, *Phys. Rev. E* **68**:056116 (2003).
48. D. B. Dougherty *et al.*, Experimental persistence probability for fluctuating steps, *Phys. Rev. Lett.* **89**:136102–136106 (2002); M. Constantin *et al.*, Infinite family of persistence exponents for interface fluctuations, *Phys. Rev. Lett.* **91**:086103 (2003); C. Dasgupta *et al.*, Survival in equilibrium step fluctuations, *Phys. Rev. E* **69**:022101 (2004).
49. M. Giesen, Step and island dynamics at solid/vacuum and solid/liquid interfaces *Prog. Surf. Sci.* **68**:1–153 (2001) and references therein.
50. R. Toussaint, G. Helgesen, and E. G. Flekkoy, Dynamic roughening and fluctuations of dipolar chains, cond-mat/0311340.
51. J. Krug *et al.*, Persistence exponents for fluctuating interfaces, *Phys. Rev. E* **56**:2702–2712 (1997); H. Kallabis and J. Krug, Persistence of Kardar–Parisi–Zhang interfaces *Europhys. Lett.* **45**:20–25 (1999); Z. Toroczkai and E. D. Williams, Nanoscale fluctuations at solid interfaces, *Phys. Today* **52**:No. 12,24–28 (1999); S. N. Majumdar and A. J. Bray, Spatial persistence of fluctuating interfaces, *Phys. Rev. Lett.* **86**:3700–3703 (2001). J. Krug, Power law in surface physics: the deep, the shallow and the useful, Physica A **340**:647 (2004).
52. H. Guclu and G. Korniss, Extreme fluctuations in small-world networks with relaxional dynamics, *Phys. Rev. E* **69**:065104(R) (2004).